



UNIVERSITY OF SCIENCE AND TECHNOLOGY OF HANOI
DEPARTMENT OF SPACE AND APPLICATIONS

PHOTONICS AND OPTICS

LECTURER: DR. PHAN THANH HIEN

Labwork Report

Duong Thu Phuong
22BI13362

Nguyen Quang Huy
22BI13197

Nguyen Ngoc Chuong
BA12-032

March 20, 2025

Contents

1 Dispersion and resolving power of the prism and grating spectroscope	5
1.1 Overview	5
1.2 Setup and Procedure	6
1.3 Theory and Evaluation	8
1.4 Results and Discussion	13
2 Michelson interferometer - high resolution	18
2.1 Overview	18
2.2 Setup and Procedure	19
2.3 Theory and Evaluation	21
2.4 Results and Discussion	24
3 Fibre optics	26
3.1 Overview	26
3.2 Setup and Procedure	27
3.3 Theory and Evaluation	29
3.4 Results and Discussion	38
4 Measuring the velocity of light	41
4.1 Overview	41
4.2 Setup and Procedure	42
4.3 Theory and Evaluation	43
4.4 Results and Discussion	44
5 Fresnel's law	46
5.1 Overview	46
5.2 Setup and Procedure	47
5.3 Theory and Evaluation	49
5.4 Results and Discussion	54
6 Helium-Neon Laser	57
6.1 Overview	57
6.2 Setup and Procedure	59
6.3 Theory and Evaluation	64
6.4 Results and Discussion	76

List of Figures

1	Experimental set-up for determining dispersion in liquids.	5
2	Set-up and path of rays in the spectrometer. (L = light source, Sp = slit in drawtube, S = collimator, SO = collimator lens, PT = prism table with adjusting screws, P = prism, FO = telescope lens, F = telescope, O = eyepiece, K = cross-wires, W = graduated circle with vernier)	6
3	Experimental set-up with vernier used auxiliary slit to determine the resolving power.	7
4	Dispersion curves of various substances	8
5	Refraction by the prism when the path of a ray is symmetrical.	9
6	Measurement of the angle of minimum deviation.	9
7	Diffraction at the grating.	11
8	Practical set-up of experiment with the glass prism	14
9	Observed spectral lines from dispersion experiment with prism	14
10	Relationship between refractive index and wavelength	15
11	Practical set-up of experiment with the grating	16
12	Spectrum of the mercury lamp using grating	16
13	Experimental set-up of the Michelson interferometer.	18
14	Setup for labwork 02.	19
15	Light path from the interferometer	22
16	Practical set-up of experiment with provided equipment	24
17	Michelson observed phenomenon.	25
18	Experimental set-up with monomode fibre (schematic).	27
19	Mounting the plug connection to module D.	28
20	Colladan's (1861) experiment for the demonstration of the total reflection of light.	30
21	Step index fibre.	31
22	Helix (A) and Meridional beam (B).	32
23	Solution of Bessel function in the core.	33
24	Focusing two beams in geometrical optics.	34
25	Beam diameter of a Gaussian beam as fundamental mode TEM00 and function of z.	35
26	Course of the radius of curvature of the wavefront as a function of the distance from the waist at $z = 0$	36
27	Rayleigh range z_r and divergence θ for the farfield $z \gg z_r$	36
28	For the calculation of the coupling optic.	37
29	Set-up and output signal	38
30	Measurements of relative output power with changing angle readout	38
31	Measurements of relative output power of diodelaser with changing injection current	39
32	Relative output power of the diode laser versus injection current	39
33	Setup for labwork 04.	42
34	Oscilloscope signal after "Calibration".	42
35	Oscilloscope signal after "Calibration".	43
36	Practical set-up of experiment with provided equipment	44
37	Practical set-up for the determination of the rotation of the plane of polarization by reflection	47

38	Experimental set up for the verification of the rotation of the plane of polarisation due to reflection (* only required for 5 mW laser)	47
39	A) direction of oscillation of the electric field vector perpendicularly and B) parallel to the direction of incidence.	49
40	Brewster's law.	51
41	Measured and calculated curves for ζ''_r and ζ'_r as a function of the angle of incidence.	52
42	Rotation of the direction of oscillation through reflection.	53
43	Measured and calculated curves for the rotation of the direction of oscillation as a function of the angle of incidence (the azimuth of the incident beam is 45°).	54
44	Reflection coefficients as a function of angle of incidence for light polarized perpendicular and parallel to the plane of incidence	55
45	Calculated curves for the rotation of the direction of oscillation as function of the angle of incidence	57
46	Leveling screws of the optical bench.	59
47	Alignment laser.	59
48	Adjustment screws.	60
49	Adjusting the alignment laser.	60
50	Correct adjusment.	60
51	Mounting the laser tube.	61
52	Adjustment of the laser tube.	61
53	Assembling the resonator mirror.	62
54	Left resonator mirror.	62
55	Cleaning tissue	64
56	Cleaning the brewster window.	64
57	Excitation and laser process for the visible laser emission.	66
58	Electron collision of the second kind.	66
59	The most important laser transitions in the neon system.	67
60	Maxwell-Boltzmann speed distribution.	69
61	Inhomogeneous line profile, speed intervals dv	70
62	Decay of the population of state 2 into state 1 and natural linewidth.	71
63	Standing longitudinal waves in an optical resonator. A with n nodes and B with $n + 3$ nodes.	72
64	Inhomogeneous gain profile (Gaussian profile) interacting with an optical resonator.	73
65	Spherical resonator with equivalent lens guide.	74
66	A: Light beam with characteristic sizes. B: Trace through a lens.	75
67	Laser tube with Brewster windows and perpendicular windows with highly anti reflection coating.	76
68	Two possible arrangements of Brewster windows.	76
69	Practical set-up of experiment	76

List of Tables

1	Equipment for labwork 01.	6
2	The dispersions and resolving powers of glass prisms determined from the dispersion curve.	11
3	Typical measurement values (diffraction of the first order) to determine the grating constant of the Rowland grating	13

4	Evaluation of the angular dispersion	13
5	Refractive indices calculation of prism	15
6	Wavelengths of the mercury spectral lines	15
7	Equipment for labwork 02.	19
8	Michelson Experiment Data	25
9	Equipment for labwork 03.	26
10	Relative output power vs injection current	39
11	Equipment for labwork 04.	41
12	Velocity of light in air	45
13	Velocity of light in acrylic glass	45
14	Velocity of light in water	45
15	Equipment for labwork 05.	46
16	Reflection coefficients for different angles of incidence	54
17	Reflection Coefficients from Theoretical Calculation	56
18	Measured and calculated curves for the rotation of the direction of oscillation .	56
19	Equipment for labwork 06.	58
20	List of accessories	58
21	Transitions and laser lines	69
22	Some special types of resonators.	75

1 Dispersion and resolving power of the prism and grating spectroscope

1.1 Overview

Principle

The refractive indices of various liquids, crown glass, and flint glass are measured based on how they bend light at different wavelengths when passing through a prism at its minimum deviation angle. Additionally, the ability of the glass prisms to distinguish between different wavelengths is evaluated using the dispersion curve.



Figure 1: Experimental set-up for determining dispersion in liquids.

Task

1. To adjust the spectrometer-goniometer.
2. To determine the refractive index of various liquids in a hollow prism.
3. To determine the refractive index of various glass prism.
4. To determine the wavelengths of the mercury spectral lines.
5. To demonstrate the relationship between refractive index and wavelength (dispersion curve).
6. To calculate the resolving power of the glass prisms from the slope of the dispersion curves.
7. Determination of the grating constant of a Rowland grating based on the diffraction angle (up to the third order) of the high intensity spectral lines of mercury.
8. Determination of the angular dispersion of a grating.
9. Determination of the resolving power required to separate the different Hg-Lines. Comparison with theory.

Equipment

Position	Material	Bestellnr.	Menge
1	PHYWE Spectrometer-Goniometer with vernier SG1 PRO	35635-03	1
2	Lamp holder pico 9 for spectral lamps	08119-00	1
3	Spectral lamp Hg 100, pico 9 base	08120-14	1
4	Power supply for spectral lamps	13662-97	1
5	Diffraction grating, 4 lines/mm	08532-00	1
6	Diffraction grating, 8 lines/mm	08534-00	1
7	Grating, 80 lines/mm	09827-00	1
8	Diffraction grating, 600 lines/mm	08546-00	1
9	Magnifier with handle, 4x, d=50 mm	87004-03	1
10	Tripod base PHYWE	02002-55	1
11	Slit, adjustable	08049-00	1
12	Barrel base PHYWE	02006-55	1
13	Right angle clamp expert	02054-00	1
14	Support rod, stainless steel, l = 250 mm, d = 10 mm	02031-00	1

Table 1: Equipment for labwork 01.

1.2 Setup and Procedure

Experiment with the glas prism

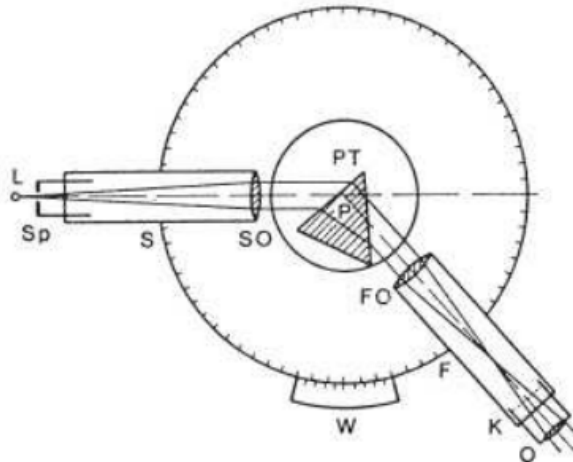


Figure 2: Set-up and path of rays in the spectrometer. (L = light source, Sp = slit in drawtube, S = collimator, SO = collimator lens, PT = prism table with adjusting screws, P = prism, FO = telescope lens, F = telescope, O = eyepiece, K = cross-wires, W = graduated circle with vernier)

The experiment is assembled as illustrated in Figure 1. The spectrometer-goniometer and diffraction grating should be adjusted according to the provided instructions. Once properly aligned, a parallel beam of light will pass through the prism, as shown in Figure 2.

To begin, the slit is aligned with the crosswires in the eyepiece, with the telescope set to infinity. The eyepiece functions as a magnifier to observe the slit. The prism is then positioned at the minimum deviation angle, and the telescope's angular position (Angle 1) is recorded from the vernier scale for each spectral line. Next, the prism is rotated so that light enters a different surface, causing the deviation to shift to the opposite side. The new angular position (Angle 2) is recorded for each spectral line at the minimum deviation angle.

To determine the wavelengths of mercury spectral lines, a ruled diffraction grating is placed perpendicularly in a holder, replacing the prism. The angles of the first-order diffracted spectral lines are measured on both the right and left sides relative to the central undeviated slit image.

The spectral lamp takes approximately 5 minutes to reach its maximum brightness. During setup, it is essential to ensure proper airflow through the ventilation slots in the lamp housing to prevent overheating.

Experiment with the grating



Figure 3: Experimental set-up with vernier used auxiliary slit to determine the resolving power.

The experimental setup is illustrated in Figure 3. First, the telescope is adjusted to focus at an infinite distance. Then, both tubes are aligned horizontally using the adjustment screws, ensuring that their axes coincide. The Hg lamp is positioned directly in front of the slit to fully illuminate it. A sharp image of the slit is projected onto the eyepiece scale and observed through the eyepiece, which acts as a magnifying lens. The slit should be set as narrow as possible for better accuracy.

Next, the grating constant of the high-resolution Rowland grating is determined. To do this, the grating is positioned perpendicular to the collimator axis and secured in place. The diffraction angles for the six most intense Hg spectral lines are measured for both first and second-order diffraction, and any visible third-order lines are also recorded. For each spectral line of the same diffraction order, the angle is measured both to the right and left of the zero-order position. Two readings are taken for each measurement using two verniers.

In higher diffraction orders, the eyepiece scale may be difficult to see due to reduced brightness. To improve visibility, a torch can be used to illuminate the grating at an angle from the telescope's direction.

To determine the resolving power of the grating, the number of illuminated grating slits is reduced. A slide caliper is placed as an auxiliary slit in front of the collimator lens. Initially, the caliper is fully closed, blocking light from reaching the grating. The slit is then gradually opened until the yellow and green Hg lines appear clearly separated. The slit width x is then reduced until the two lines are just distinguishable. The average slit width is recorded over multiple trials. Gratings with up to 50 lines/mm are used to determine the resolution required for separating the yellow-green lines. The Rowland grating is specifically used to separate the closely spaced yellow Hg lines.

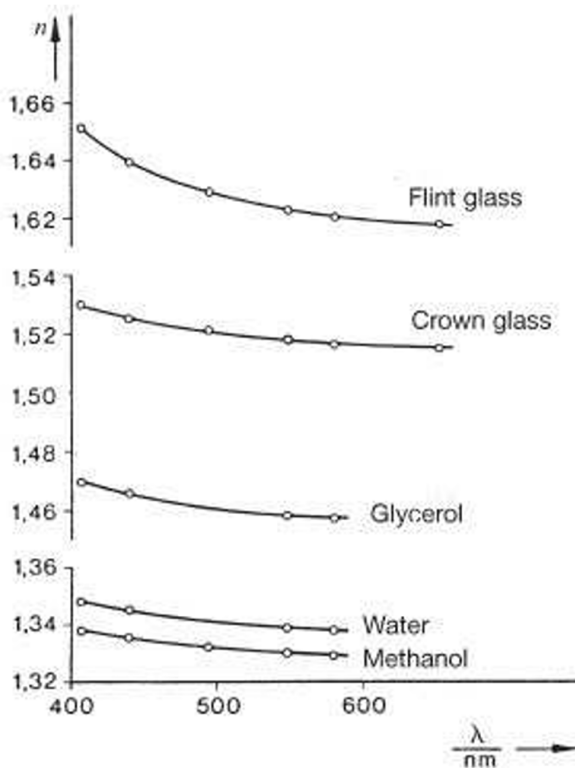


Figure 4: Dispersion curves of various substances

1.3 Theory and Evaluation

Dispersion and resolving power of the prism

The refractive index of a medium is linked to the relative permittivity ϵ_r by the Maxwell relationship

$$n = \sqrt{\epsilon_r \mu_r} \quad (1)$$

For most substances the permeability is: $\mu_r = 1$

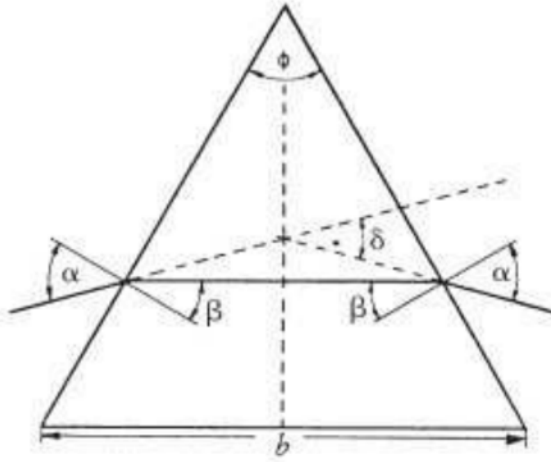


Figure 5: Refraction by the prism when the path of a ray is symmetrical.

According to Clausius and Mossotti, there exists the following relationship between the relative permittivity and the molecular polarizability α of a medium:

$$\alpha = \frac{3\epsilon_0 \epsilon - 1}{N \epsilon + 2} \quad (2)$$

where N is the concentration of the polarizable molecules and ϵ is the electric field constant.

The polarizability of a substance is dependent on the frequency $\omega = 2\pi\nu$ of the incident light. Beyond the natural frequency $\omega_0 = 2\pi\nu_0$ of an atom or molecule, the following approximation holds true:

$$\alpha = \frac{e^2}{m} \frac{1}{\omega_0^2 - \omega^2} \quad (3)$$

where e is the elementary charge and m is the mass of an electron.

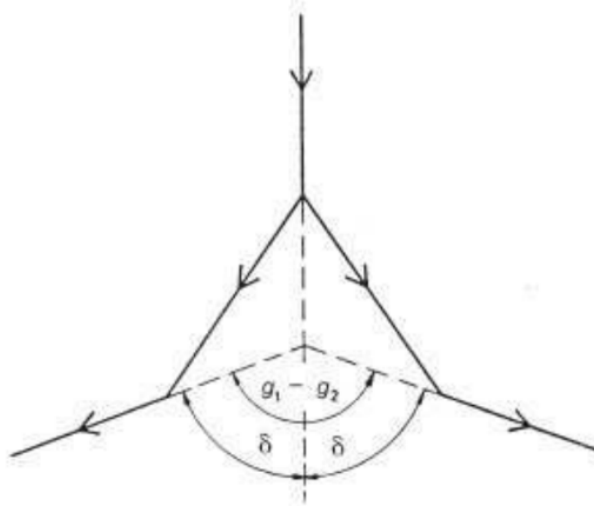


Figure 6: Measurement of the angle of minimum deviation.

When 1 and 3 are substituted in 2 we obtain

$$\frac{n^2 - 1}{n^2 + 1} \frac{e^2 N}{3\epsilon_0 m} \frac{1}{\omega_0^2 - \omega^2} \quad (4)$$

Although equation 4 considers only one natural frequency, it effectively describes the decrease in the refractive index as the wavelength increases outside the range of natural frequencies.

The spectral lines' wavelengths are determined using a diffraction grating, which is positioned in the path of the light rays, rather than a prism. For a wavelength λ , a grating constant G , and an angle ϕ at which the first order diffraction pattern appears, the following applies: $\lambda = G \cdot \sin \phi$.

λ is determined from the average of several measurements:

- $\lambda_{red} = 627.3\text{nm}$
- $\lambda_{yellow} = 579.8\text{nm}$
- $\lambda_{green} = 547.7\text{nm}$
- $\lambda_{turquoise} = 493.9\text{nm}$
- $\lambda_{blue} = 438.5\text{nm}$
- $\lambda_{violet} = 405.1\text{nm}$

When light travels symmetrically through a prism (as shown in Fig. ??), it undergoes minimal deviation, denoted as δ . If α represents the angle of incidence, β denotes the angle of reflection, and θ indicates the angle of the prism, then $\sin \alpha = n \sin \beta$

$$\beta = \frac{\theta}{2} \text{ and } \delta = 2\alpha - \theta \quad (5)$$

From these we obtain

$$n = \frac{\sin \frac{\theta + \delta}{2}}{\sin \frac{\theta}{2}} \quad (6)$$

The angle of minimum deviation δ is obtained from the difference between the angles ϕ_1 and ϕ_2 measured at the two different prism position (Fig. ??): $\delta = \frac{\phi_1 - \phi_2}{2}$.

The dispersion curve is determined from the angles measured for the various mercury spectral lines.

The effectiveness of a spectrometer is measured by its 'resolving power'. This means it can still differentiate between two wavelengths, λ and $\lambda + d\lambda$, even if the highest point of wavelength $\lambda + d\lambda$ lines up with the lowest point of wavelength λ . Resolving power, denoted as R , is generally defined using a specific formula: $R = \frac{\lambda}{d\lambda}$.

For a prism, the following applies: $R = b \cdot \left| \frac{dn}{d\lambda} \right|$ where b is the base of the prism.

Resolving power R is determined in the ‘yellow’ and the ‘blue’ regions of the spectrum from the slope of the dispersion curve with the prism fully illuminated ($b = 30\text{mm}$).

Spectral region: yellow	$\frac{dn}{d\lambda}/\text{cm}^{-1}$	$\frac{\lambda}{d\lambda}$
Flint glass	691	2073
Crown glass	377	1131
Spectral region: blue	$\frac{dn}{d\lambda}/\text{cm}^{-1}$	$\frac{\lambda}{d\lambda}$
Flint glass	2365	7095
Crown glass	1126	3378

Table 2: The dispersions and resolving powers of glass prisms determined from the dispersion curve.

Dispersion and resolving power of a grating

If monochromatic light with the wavelength λ impinges on a diffraction grating, the intensity diffracted according to the angle ϕ given by:

$$I(\phi) = I(0) \cdot I(\phi) = I(0) = \left(\frac{\sin u}{u}\right)^2 \left(\frac{\sin Nv}{\sin v}\right)^2$$

with $v = \pi \frac{g}{\lambda}$ and $u = \pi \frac{s}{\lambda}$ (7)

(s = width of the slit; g = distance between two slits = grating constant, N = number of slits).

We have:

$$AB - CD = g(\sin \beta - \sin \alpha) = z\lambda$$

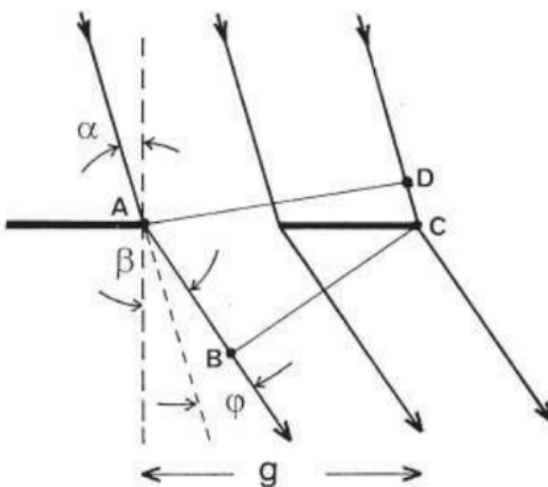


Figure 7: Diffraction at the grating.

The first bracket describes the distribution of intensities due to diffraction by a single slit, whereas the combined effect of all the slits is described by the second bracket. If one bracket

is zero, then total intensity $I(\phi) = 0$. This means however, that minima due to a single slit continue to exist when N slits act together. On the other hand, peaks due to a single slit can be interspersed by further secondary minima if the second bracket is zero.

The diffraction direction ϕ of maximum z for a given grating fulfils the following relation:

$$v_z = \pi \frac{g}{\lambda} \sin \phi_z = z\pi \text{ or } \sin \phi_z = z \frac{\lambda}{g}$$

$$z = \text{order of diffraction} = \pm(0, 1, 2, \dots) \quad (8)$$

There are $(N-1)$ secondary minima between every two peaks. If light impinges at an angle α against the perpendicular to the grating, the following is valid.

$$\sin \phi + \sin \beta = \frac{-\lambda}{9} = 2 \sin \frac{\alpha + \beta}{2} \cdot \cos \frac{\alpha - \beta}{2} = 2 \sin \frac{\phi}{2} \cos \frac{\alpha - \beta}{2} \quad (9)$$

with $\beta - \alpha = \phi$.

The angle β is considered to be positive when the diffracted and incident beams are on the same side of the perpendicular to the grating. If each angle is on another side of the perpendicular, then β is negative. In case of perpendicular incidence ($\alpha = 0$), the following applies:

$$\sin \phi = z \frac{\lambda}{g} \quad (10)$$

By differentiation of one obtains the angle of dispersion $d\phi/d\lambda$ of the grating:

$$\frac{d\phi}{d\lambda} = \frac{z}{g \cos \beta} = \frac{z}{g \cos \phi} \text{ (with } \beta = \phi, \text{ if } \alpha = 0) \quad (11)$$

Angular dispersion is independent of the angle of incidence and compared to prisms, it remains nearly constant for small diffraction angles.

Two spectral lines λ_1 and λ_2 only can be separated if they are so far apart from each other that the peak of λ_1 coincides with the minimum of λ_2 (Rayleigh criterion). The quotient of the average wavelength and the difference between the wavelengths of lines which merely appear separated is called the spectral resolving power:

$$A = \frac{0.5(\lambda_1 + \lambda_2)}{\lambda_2 - \lambda_1} = \frac{\bar{\lambda}}{\Delta \lambda} \quad (12)$$

The following is valid for the spectral resolving power of a diffraction grating:

$$A = z \cdot N \quad (13)$$

(z = order of diffraction; N = effective (illuminated) number of slits).

Table 3 shows the results (for $z = \pm 1$) of a typical measurement for the determination of grating constant g . The diffraction angle ϕ of a spectral line is calculated from the half angular difference of the corresponding diffraction order $\pm z$. Finally, as two values $\phi(1)$ and $\phi(2)$ are determined for every angle due to the two verniers, the average value is:

$$\bar{\phi} = 1/4 [(\phi(1)_{+z} - \phi(1)_{-z}) - (\phi(2)_{+z} - \phi(2)_{-z})]$$

No.	Colour	N/hm	$\phi(1)$	$\phi(2)$	$\phi(1)$	$\phi(2)$	ϕ	g/um
			$z = +1$	$z = +1$	$z = -1$	$z = -1$		
1	viol.	404.656	253°56'	73°56'	225"40'	45°43'	14.12*	1.6586
2	blue	435.405	255°05'	75°06'	224°35'	44°38'	15.24°	1.6562
3	bl.-	491.604	257°06'	77'07'	222°34*	42°39'	17.25°	1.6578
4	green	546.074	250°06'	79°08'	220°37'	40°41'	19.23°	1.6577
5	yellow	576.960	260°15'	80°16'	219°28'	39°34'	20.37°	1.6575
6	yellow	578.966	260°20'	80°20'	219°23'	39°27'	20.46°	1.6565

Table 3: Typical measurement values (diffraction of the first order) to determine the grating constant of the Rowland grating

If one also considers the refraction of lines No.1-No. 6 in the second order ($z = \pm 2$), as well as those third order lines ($z = \pm 3$) which still can be recognised, the grating constant is found to be:

$$g = (1.6567 \pm 0.0016)\mu\text{m}; \quad \Delta g/g = \pm 0.1\%; (603.6 \pm 0.6)/\text{mm}.$$

According to (11) ($z = \pm 1$; d must be converted to radian for assessment. The values $d\phi$ and $d\lambda$ are obtained from the difference between the corresponding values of neighbouring lines).

No.	λ/nm	$\phi/^\circ$	$d\lambda/\text{nm}$	$d\phi/\text{rad}$	$(d\phi/d\lambda)\text{m}^{-1}$	$(g \cos \phi)^{-1}/\text{m}^{-1}$
1	404.656	14.12				
2	435.405	15.24	30.75	0.01955	6.36×10^5	6.22×10^5
3	491.604	17.25	56.20	0.03490	6.21×10^5	6.28×10^5
4	546.074	19.23	54.50	0.03490	6.40×10^5	6.35×10^5
5	576.960	20.37	30.90	0.01989	6.44×10^5	6.41×10^5
6	578.966	20.46	2.00	0.00152	7.56×10^5	6.44×10^5

Table 4: Evaluation of the angular dispersion

A theoretical resolving power $A = 562 \text{ nm}/32 \text{ nm} = \sim 17.6$ is required to separate the green Hg-line- $\lambda_1 \sim 546 \text{ nm}$ from the pair of yellow lines $\lambda_2 \sim 578 \text{ nm}$. To separate the two yellow Hg-lines $\lambda_1 = 576.960 \text{ nm}$ and $\lambda_2 = 578.966 \text{ nm}$, A must at least be 289.

1.4 Results and Discussion

Experiment setup using glass prism

The figures below illustrate the spectrum emitted by the Hg lamp used in the experiment.



Figure 8: Practical set-up of experiment with the glass prism

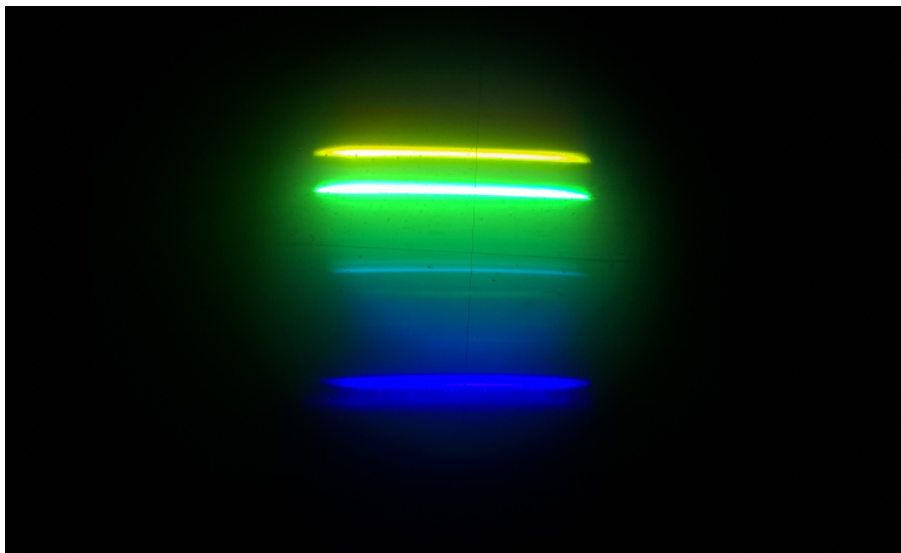


Figure 9: Observed spectral lines from dispersion experiment with prism

Refractive index of glass prism

From Eq.5, we know that the angle of the prism θ is 60° , then we can calculate the angle of reflection:

$$\beta = \frac{\theta}{2} = \frac{60^\circ}{2} = 30^\circ \quad (14)$$

And thus, the refractive index of the prism can be calculated as:

$$n = \frac{\sin \alpha}{\sin \beta} \quad (15)$$

The only parameters we need to measure are the angle of incidence α for each wavelength. Then we substitute these measurements into the above equation to obtain the corresponding refractive indices.

The results are shown in the table below.

Spectral line	Incidence angle α	Refractive index n
Red	50.1°	1.577
Yellow	50.33°	1.584
Green	50.66°	1.59
Turquoise	51.32°	1.597
Blue	52.32°	1.618

Table 5: Refractive indices calculation of prism

Wavelengths of the mercury spectral lines

The value λ is determined from the average of several measurements:

Spectral line	Wavelength λ (nm)
Red	627.3
Yellow	579.8
Green	547.7
Turquoise	493.9
Blue	438.5
Violet	405.1

Table 6: Wavelengths of the mercury spectral lines

Relationship between refractive index and wavelength

Based on the two results above, we can easily plot the relationship between the refractive index and the wavelengths using Python.

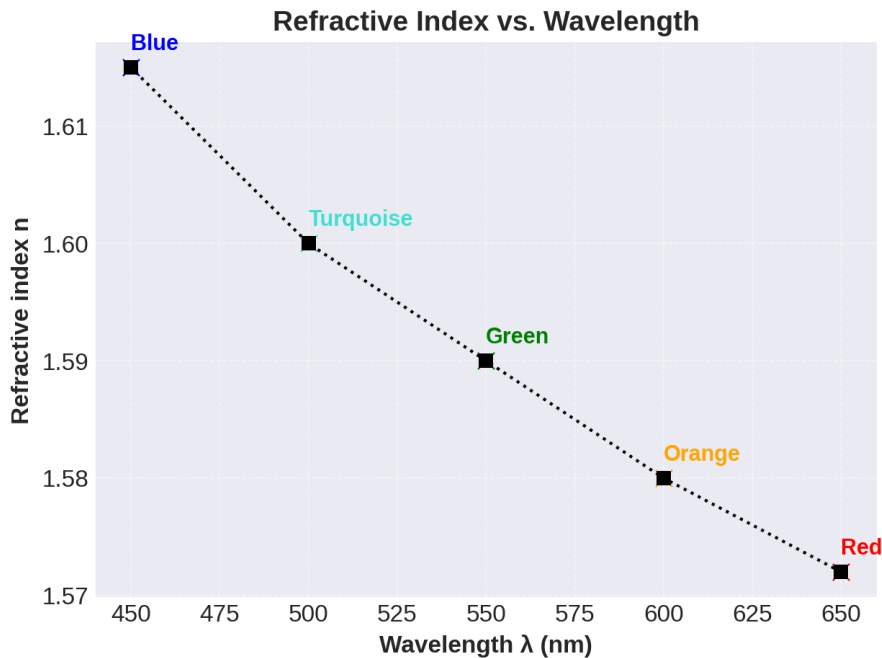


Figure 10: Relationship between refractive index and wavelength

Figure 10 illustrates the dispersion curve of the glass prism used in our experiment. As shown, the data points do not align perfectly with the curve, which can be attributed to human error and distortion from external light sources.

Resolving power of the prism from the slope of the dispersion curves

Using Figure 4 and our own results as shown above, we can identify that the prism is made from crown glass. Then, using Table 2, we can conclude that the resolving power R is approximately

Spectral region: yellow	$\frac{dn}{d\lambda} / \text{cm}^{-1}$	$\frac{\lambda}{d\lambda}$
Prism	400	2400
Spectral region: blue	$\frac{dn}{d\lambda} / \text{cm}^{-1}$	$\frac{\lambda}{d\lambda}$
Prism	1200	7200

Experiment setup using grating



Figure 11: Practical set-up of experiment with the grating

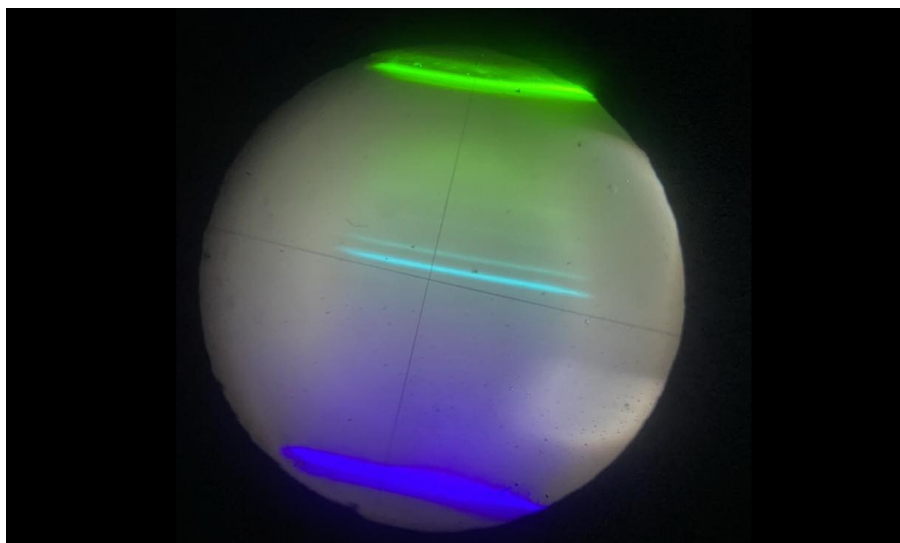


Figure 12: Spectrum of the mercury lamp using grating

Grating constant of the Rowland grating

In this experiment, we measured the refraction angles for different wavelengths according to their diffraction order z (Fig. 12):

- $\beta_{\text{red}_1} = 99.33^\circ$
- $\beta_{\text{red}_2} = 99.6^\circ$
- $\beta_{\text{yellow}_1} = 98.33^\circ$
- $\beta_{\text{yellow}_2} = 98^\circ$
- $\beta_{\text{green}_1} = 97.26^\circ$
- $\beta_{\text{green}_2} = 113.96^\circ$
- $\beta_{\text{turquoise}_1} = 96^\circ$
- $\beta_{\text{turquoise}_2} = 96.66^\circ$
- $\beta_{\text{blue}_1} = 93.96^\circ$
- $\beta_{\text{blue}_2} = 105.94^\circ$

In this setup (Fig. 43), the incident angle is set to $\alpha = 40^\circ$. Using the diffraction equation:

$$g(\sin \beta - \sin \alpha) = z\lambda \quad (16)$$

where g is the grating constant and z represents the diffraction order.

By substituting the corresponding values, we determine the grating constant to be approximately $g \sim 1.824 \text{ } (\mu\text{m})$.

Angular dispersion of a grating

According to Eq.11, the angular dispersion $\frac{d\phi}{d\lambda}$ can be easily determined from the measurements of the diffraction angle.

Using the data from the previous task, we determine the angular dispersion as

$$\frac{d\phi}{d\lambda} = 3.637 \text{ } \mu\text{m}^{-1}.$$

Resolving power required to separate the different Hg-lines

Using the formula 12, a theoretical resolving power $A = 562 \text{ nm}/32 \text{ nm} \approx 17.6$ is required to separate the green Hg-line $\lambda_1 \approx 546 \text{ nm}$ from the pair of yellow lines $\lambda_2 \approx 578 \text{ nm}$. To separate the two yellow Hg-lines $\lambda_1 = 576.960 \text{ nm}$ and $\lambda_2 = 578.966 \text{ nm}$, A must be at least 289. Table 2 gives the averages of the auxiliary slit width x obtained over several measurements, which are necessary to separate the lines of different diffraction orders z for various gratings. The last three columns give the values for the corresponding resolving power A .

Separation of the green Hg-line from the pair of yellow lines						
Lattice	$z = 1$	$z = 2$	$z = 3$	$A(z = 1)$	$A(z = 2)$	$A(z = 3)$
4/mm	-	$x = 2.32 \text{ mm}$	-	-	18.6	-
8/mm	$x = 2.27 \text{ mm}$	$x = 1.09 \text{ mm}$	-	18.2	17.4	-
10/mm	$x = 1.80 \text{ mm}$	$x = 0.84 \text{ mm}$	$x = 0.58 \text{ mm}$	18.0	16.8	17.4
50/mm	$x = 0.35 \text{ mm}$	-	-	17.5	-	-

Separation of the yellow Hg-lines						
603.6/mm	$x = 0.475 \text{ mm}$	-	-	287	-	-

The experimentally determined average values of A needed to separate the yellow-green and yellow-yellow lines, measured as 17.7 and 287 respectively, align well with the theoretical predictions.

2 Michelson interferometer - high resolution

2.1 Overview

Principle

Using two mirrors in a Michelson configuration, light is made to interfere. As one of the mirrors is moved, changes in the interference pattern are observed, allowing the wavelength of the laser light to be measured.



Figure 13: Experimental set-up of the Michelson interferometer.

Task

1. Construction of a Michelson interferometer using separate components.
2. The interferometer is used to determine the wavelength of the laser light.
3. The contrast function K is qualitatively recorded in order to determine the coherence length with it.

Equipment

Position No.	Material	Order No.	Quantity
1	Optical base plate 450 × 600 mm	08750 – 00	1
2	He-Ne Laser, 632 nm, 1 mW, linear polarised	08182 – 93	1
3	Surface mirror 30 × 30 mm	08711 – 01	4
4	Accessory set for optical base plate	08750 – 50	1
5	Holder for diaphragms and beam splitters	08719 – 00	1
6	Beam splitter 1/1, non polarizing	08741 – 00	1
7	Lens, mounted, f + 20 mm	08018 – 01	1
8	Lensholder for optical base plate	08723 – 00	1
9	Screen, white, 150 × 150 mm	09826 – 00	1
10	linear translation stage, 25 mm	08750 – 09	1
11	Photoelement	08734 – 00	1
12	Digital multimeter 2005	07129 – 00	1
13	Measuring tape, I = 2 m	09936 – 00	1
14	Adjusting support 35 × 35 mm	08711 – 00	4

Table 7: Equipment for labwork 02.

2.2 Setup and Procedure



Figure 14: Setup for labwork 02.

The experimental setup is illustrated in Figure 14, serving as a general reference. The recommended beam path height is 120 mm, which can be maintained using a ruler to measure and align each optical component as they are placed on the base plate.

Important Notes:

- Once an optical component is mounted on a support and positioned correctly, it should be securely clamped to prevent any unintended movement.
- Caution: Never look directly into an unattenuated laser beam. The lens L should not be in place during the initial alignment.

Beam Path Adjustment

The beam path is first aligned using the adjustable mirrors M1 and M2, ensuring it travels straight along the base plate until it reaches mirror M3. This initial alignment is performed without the beam splitter BS.

Mirror M3 is mounted on a linear translation stage. It is adjusted (still without BS) so that the reflected beam returns to the same point on mirror M2 from which it originated.

Next, the beam splitter BS is inserted into the beam path with its metallized side facing M2, ensuring that one partial beam continues towards M3 without deviation, while the other is reflected perpendicularly to mirror M4. The beam reflected from M4 is then adjusted using fine screws to align with the same point on the screen SC as the beam reflected from M3 via the beam splitter. A slight flickering of the overlapping light spots indicates that the alignment is nearly perfect.

When lens L is placed in the beam path, the light spots expand, making interference patterns (such as stripes or concentric circles) visible on screen SC. By carefully adjusting mirrors M3 and M4, well-defined concentric circles can be observed.

Determining the Wavelength of Laser Light

To measure the laser wavelength, the optical path length between mirror M3 and the beam splitter BS is altered. This is achieved by shifting mirror M3 using a lever arm (lever ratio 20:1) and a micrometer screw (where two turns correspond to a 1 mm shift). As the optical path length changes, the interference pattern at the center of the rings shifts between maxima and minima.

The direction of the shift reveals whether the path length is increasing or decreasing:

- If the center alternates between bright and dark, the path length is decreasing.
- If the center behaves oppositely, the path length is increasing.

According to theoretical principles, a complete shift from one minimum to the next occurs when the optical path length changes by one wavelength. Therefore, by measuring the displacement of M3 (initial and final values on the micrometer screw) and counting the number of alternating minima and maxima, the laser wavelength can be determined.

Recording the Contrast Function

For contrast function measurement, screen SC is replaced with a photocell PD to capture intensity variations. To ensure precise readings, black tape is used to narrow the slotted diaphragm to an aperture of approximately 1 mm^2 , preventing the photocell from detecting interference across multiple maxima and minima.

To minimize background noise, the experiment should be conducted in a darkened room, reducing the photocell's dark current. The contrast function is determined by measuring intensity variations of minima and maxima while adjusting the mirror separation. Only mirror M4 should

be moved during this step, and it must remain on a straight path.

To record the distance between mirrors and the beam splitter, a measuring tape is used. Each time the mirror is repositioned, realignment may be necessary to ensure interference fringes remain visible. Using a micrometer screw, M3 is slightly adjusted to find the maximum and minimum voltage values, which are then measured with a multimeter (range 500 mV).

The optical path difference between the two mirrors and the beam splitter should be varied between 0 and 10 cm. When M3 is $\sim 13\text{cm}$ from BS, M4 should be positioned between 8 cm (minimum separation) and 13 cm (maximum separation) from BS.

At larger separation differences, the radii of the interference rings decrease, making the measurement of maximum and minimum intensities less precise. Additionally, the relatively large diaphragm aperture introduces significant measurement errors at these distances.

2.3 Theory and Evaluation

Wave Superposition and Interference

If two waves with the same frequency but different amplitudes and phases coincide at the same location, they superimpose as:

$$E(t) = A_1 \cdot \sin(\omega t - \phi_1) + A_2 \cdot \sin(\omega t - \phi_2) \quad (17)$$

The resulting wave can be expressed as:

$$E(t) = A \cdot \sin(\omega t - \phi) \quad (18)$$

where the amplitude is given by:

$$E^2(t) = A_1^2 + A_2^2 + 2 \cdot A_1 \cdot A_2 \cdot \cos \delta \quad (19)$$

and the phase difference:

$$\delta = \phi_1 - \phi_2 \quad (20)$$

Interference in a Michelson Interferometer

In a Michelson interferometer, light is split by a semi-transparent glass plate into two partial beams (amplitude splitting). These beams are reflected by two mirrors and brought back to interfere behind the glass plate (see Fig. 2). Since only extended luminous spots can form circular interference fringes, the light beam is expanded using lens L .

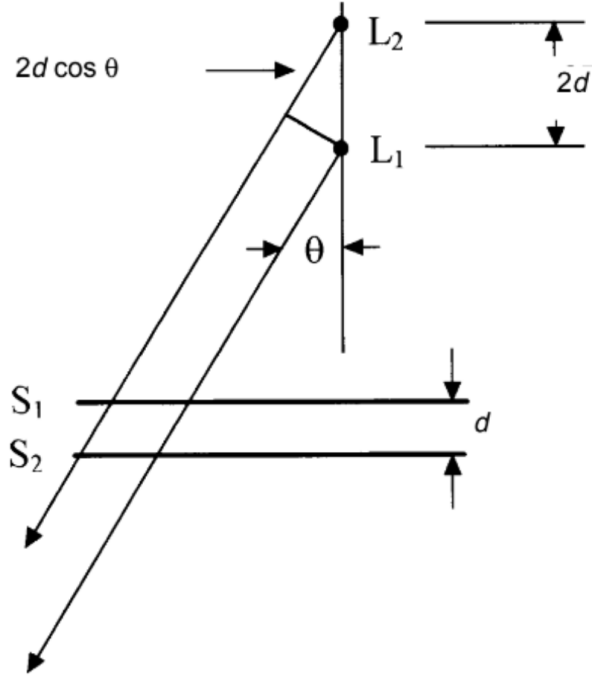


Figure 15: Light path from the interferometer

Due to differences in optical path lengths, the phase difference is given by:

$$\delta = \frac{2\pi}{\lambda} \cdot 2 \cdot d \cdot \cos \theta \quad (21)$$

For equal amplitudes $A_1 = A_2 = A$, the intensity distribution is:

$$I = E^2 = 4A^2 \cos^2 \frac{\delta}{2} \quad (22)$$

Maxima occur when:

$$2 \cdot d \cdot \cos \theta = m \cdot \lambda, \quad m = 1, 2, \dots \quad (23)$$

Thus, circular fringes appear for fixed values of m and d , which remain constant. If the movable mirror M_3 is adjusted such that d decreases, the circular fringe diameter also shrinks. A fringe disappears each time d is reduced by $\lambda/2$. At $d = 0$, the interference pattern disappears. If mirrors M_3 and M_4 are not perfectly parallel, curved fringes form, transitioning to straight fringes at $d = 0$.

Determining the Wavelength of Light

To measure the wavelength of light, the number of circular fringe shifts is counted while moving mirror M_3 using a micrometer screw (transmission ratio 20:1):

$$\lambda = \frac{2d}{N} \quad (24)$$

where λ is the wavelength, d is the displacement, and N is the number of fringes passing a point.

Temporal Coherence and Contrast Function

The temporal coherence (coherence time and length) of a laser can be measured using a Michelson interferometer. Due to differing optical path lengths in the interferometer, the split laser beam experiences a temporal delay before interfering with itself. The coherence time represents the delay at which the wave trains can still interfere:

$$\tau < \tau_c \quad (25)$$

$$l_c = c \cdot \tau_c \quad (26)$$

where c is the speed of light. The resonator determines the laser's oscillation modes via its resonance condition:

$$L_R = n \frac{\lambda}{2}, \quad n = 1, 2, 3, \dots \quad (27)$$

Only frequencies within the emission spectrum of the gain medium and above the threshold of resonator losses are allowed.

Auto-correlation and Contrast Measurement

The contrast between bright and dark fringes in the interference pattern measures the coherence of light. This can be determined using the auto-correlation function:

$$I = (E \cdot E^*) \quad (28)$$

where E^* is the complex conjugate of E . In the Michelson interferometer:

$$I_{\text{res}} = ((E_1 + E_2) \cdot (E_1 + E_2)^*) \quad (29)$$

Since E_1 and E_2 are identical except for a time shift τ :

$$E_2(t) = E_1(t + \tau) \quad (30)$$

$$\Gamma(\tau) = (E(r) \cdot E^*(t + \tau)) \quad (31)$$

$\Gamma(\tau)$ is the auto-correlation function, also called the self-coherence function. The resulting intensity is:

$$I_{\text{res}} = 2I + 2\text{Re}(\Gamma(\tau)) \quad (32)$$

The interference pattern contrast is given by:

$$K = \frac{I_{\max} - I_{\min}}{I_{\max} + I_{\min}} \quad (33)$$

The normalized self-coherence function is the complex degree of self-coherence:

$$\gamma(\tau) = \frac{\Gamma(\tau)}{\Gamma(0)} \quad (34)$$

For a monochromatic plane wave propagating in the x -direction:

$$K = |\gamma(\tau)| = 1 \quad (35)$$

which implies infinite coherence length in an ideal case. However, in reality, coherence length is limited by natural line width (in gas lasers, also by Doppler broadening).

For a laser oscillating in two modes at frequencies ω_1 and ω_2 :

$$\Gamma(r) = ((E_1(t) + E_2(t)) \cdot (E_1(t + \tau) + E_2(t + \tau))^*) \quad (36)$$

$$= \Gamma_1(\tau) + \Gamma_2(\tau) \quad (37)$$

$$= |A_1|^2 e^{-i\omega_1\tau} + |A_2|^2 e^{-i\omega_2\tau} \quad (38)$$

For equal amplitudes $A_1 = A_2$ and $\omega_2 = \omega_1 + \Delta\omega$, the contrast function is:

$$K = |\gamma(\tau)| = \cos\left(\frac{\Delta\omega \cdot \tau}{2}\right) \quad (39)$$

For a laser with 5 mW power and a resonator length of approximately 30 cm, the frequency separation of axial modes is:

$$\Delta\omega = 2\pi \cdot \frac{c}{2L} = (3.1 \text{ GHz}) \quad (40)$$

The propagation delay due to mirror displacement is:

$$\tau = \frac{2d}{c} \quad (41)$$

Thus, the contrast function simplifies to:

$$K = \cos\left(\frac{\pi d}{L}\right) \quad (42)$$

2.4 Results and Discussion

Experiment setup

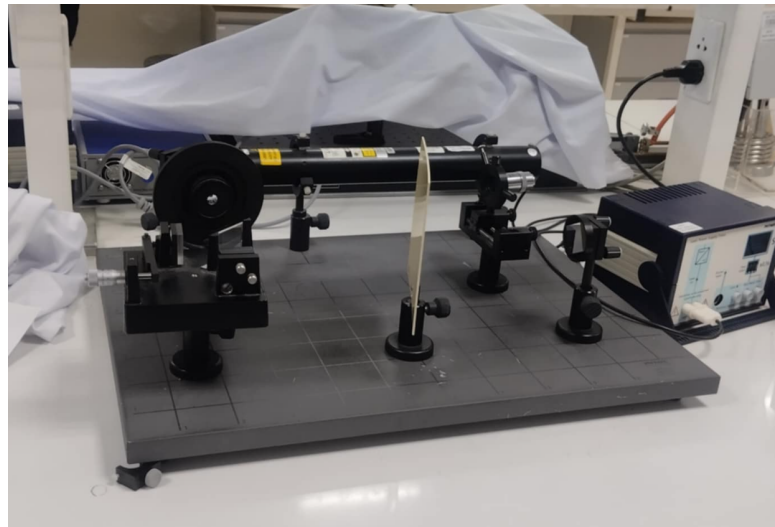


Figure 16: Practical set-up of experiment with provided equipment

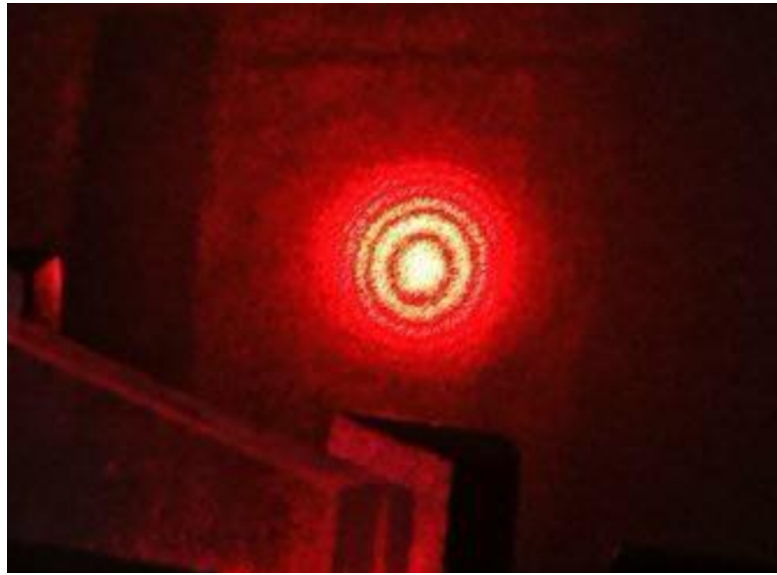


Figure 17: Michelson observed phenomenon.

Determining the wavelength

To determine the wavelength of light, observe the circular fringe shifts while adjusting the mirror using the micrometer screw (with an approximate transmission ratio of 20:1).

During the process, the mirror is shifted by $0.1\text{mm} = 100\mu\text{m}$, and a total of $N = 29$ circular fringe transitions are recorded.

$$\lambda = \frac{2 \cdot d}{N} = \frac{2 \cdot 100\mu\text{m}}{29}$$

Using these values, the calculated wavelength of light is $\lambda = 6.89 \mu\text{m}$.

To minimize errors, this procedure is repeated with varying distances, and the results are presented in the following table:

Test No	$d (\mu\text{m})$	N	$\lambda (\mu\text{m})$
1	100	29	0.689
2	80	25	0.640
3	60	19	0.631
4	40	12	0.666

Table 8: Michelson Experiment Data

Taking the average of all calculations, we obtain the wavelength as $\lambda = 0.652 \mu\text{m}$.

Contrast Function K and Coherence Length

Due to the lack of several essential instruments, we were unable to gather sufficient data required for calculations. Consequently, further experimentation could not be conducted.

3 Fibre optics

3.1 Overview

Equipment

Position No.	Material	Item No.	Quantity
1	Screened cable, BNC, $l = 750$ mm	07542-11	2
2	Digital storage oscilloscope, 20 MHz 2 channels, 100 MS/s	EAK-P-1335	1
3	Experimental set Fibre optics	08662-93	2

Table 9: Equipment for labwork 03.

Task

1. For coupling the diodelaser beam into the fibre, the beam is first collimated by means of Module B. The distance of Module C to Module B is more or less arbitrary since the laser beam is nearly parallel. 50 mm are recommended. Now the fibre adjustment holder (Module D without fibre) is put on the rail at a distance of about 10 mm from Module C. The fibre is then carefully mounted to the fibre adjustment holder and inserted.

The laser diode is switched to maximum injection current and the internal modulation is “on”. The detector is fixed to the holder plate G in front of the fibre exit. If the amplifier of the control unit and the oscilloscope are set to highest amplification, one already detects modulated laser light at the exit of the fibre. Now the fibre has to be adjusted.

While observing the amplitude on the oscilloscope one turns gently the XY and Θ , Φ adjustment screws of the adjustment holder. If there is no further increase in the amplitude the distance between fibre and coupling optics will be changed by acting on the linear displacement of the sliding mount.

In the new position the adjustment screws are readjusted. Since the amplitude increases continuously the amplification of the oscilloscope has to be reduced accordingly. At a certain state of adjustment the injection current has to be reduced since meanwhile so much power is coupled to the fibre that the detector approaches saturation.

By means of the IR conversion card one can now observe the outgoing radiation if the room is sufficiently darkened. The previous adjustment steps are repeated until no further power increase is observed. The set-up is now well prepared for the following measurements.

2. The control unit LDC01 has a modulation input to which a signal generator can be connected. That way the injection current can be modulated by any type of LF – signal. The signal generator should have an adjustable off-set to get the working point in the midst of the characteristic line of the laserdiode. Any source of signals can be used as a signal generator, also sources of digital signals, provided they have the required input voltage level.

3. The holder G with the PIN photodiode is positioned on the right rail at a distance not too far from holder E predetermined by the rotation joint. The output power of the fibre is measured for different angles from -10 to +10 degree. We use modulated light to eliminate the influence of environmental disturbances. The amplitudes are proportional to the light intensity.

4. Another very interesting experiment is the measurement of the transit time of light through the fibre. The set-up is modified so that the detector is again next to the end of the fibre in holder G. The detector is connected directly to the oscilloscope of 100 MHz. To reduce the rise time of the signal a 50Ω resistor is used as shunt. The second channel is connected to the monitor exit of the injection current at the control unit LDC01.

For an appropriate set of time base one gets curve A on the second channel. The fibre is now eliminated from the set-up by taking off the mounted plug connections from the holders. (Attention! Put the fibre ends in a safe place).

Curve B is represented on the first channel and the time difference T1 at 50 % of the rise time is measured. The time T1 represents all transit time delays of the system without fibre. Then the fibre is reinserted and adjusted to maximum power.

Next we are going to find curve C and time T2. The time T2 contains the transit time delays of the system and the transit time of the light through the fibre.

5. The PIN photodiode is now placed at a distance of 2 cm in front of the diodelaser. The supply current of the diodelaser is modulated internally. After ensuring that the photodiode is not saturated the relative output power of the diodelaser is measured for increasing values of the supply current.

3.2 Setup and Procedure



Figure 18: Experimental set-up with monomode fibre (schematic).

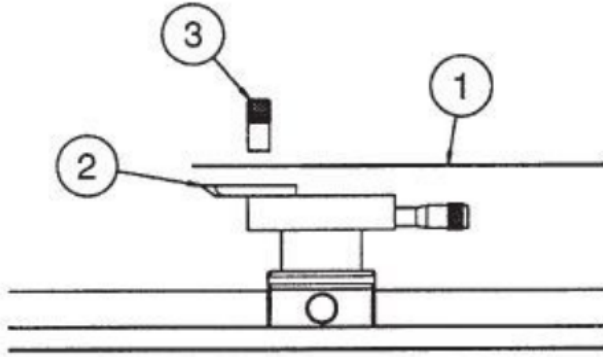


Figure 19: Mounting the plug connection to module D.

After eliminating the insulation from both fibre ends by scratching, the cut and cleaved fibre is to put into the groove of holder and carefully fixed with the magnet.

Module A: The laser diode in its housing is mounted on a XYfine adjustment. A Peltier cooler and a thermistor for measuring the laser diode temperature are incorporated in the housing. The laser diode emits a maximum power of 50 mW.

Module B: A microscope objective collimates the laser diode radiation. The objective is screwed into the mounting plate that it can easily be removed from the plate holder and exchanged for another one. Before we start with the measurements we have to define the optical axis of the set-up. This is done with the help of an oscilloscope. The injection current is modulated so that we can see rectangular pulses on the oscilloscope. The collimator (Module B) is brought at such a position to the laser diode that a nearly parallel laser beam is formed.

Module B: By means of the XY-displacement screws of Module A the laser beam is then centralised on the detector. This can be checked by looking for the maximum signal on the oscilloscope. Precaution has to be taken that the detector does not reach saturation. Eventually the injection current has to be reduced by a suitable amount. The next step is to bring the coupling optics (Module C) into the set-up.

Module C: Basically the same arrangement as Module B but with a fine adjustment holder with four axis XY, Θ and Φ and an objective of smaller focal distance to focus the collimated laser diode radiation in such a way that an effective coupling to the fibre is ensured. A beam shaping of the laser diode radiation has purposely been omitted to simplify the entrance into the experiment.

Module D: Before starting the experiment the prepared fibre is mounted to the Module D. The fibre holder is mounted on a stage with linear displacement in the direction of the beam.

Module F: 100 m monomode fibre are coiled up on a drum. Of course multimode fibres can also be used, which make alignment much easier.

Module E: On a hinged joined angle connector the second fibre holder is mounted, but without a linear stage. This device allows the measurement of the angle dependent output power of the

fibre.

Module G: This module consists of the detector with a PIN photodiode. The connection to the preamplifier of the control unit LDC01 is made by a BNC cable. The inner pin of the BNC plug is in contact with the anode of the photodetector.

3.3 Theory and Evaluation

One essential desire of human beings is to use information faster than others for their own benefit. In his publication “Die Quasioptik der Ultrakurzwellenleiter” H. Buchholz expressed in 1939 the idea to guide light signals along light – conducting material and to use them for data transmission. But only with the development of the semiconductor laser in 1962 was Buchholz’ idea materialised by using just these lasers and fibres as a light transmitting medium.

Suddenly, simple and powerful light sources for the generation and modulation of light were available. Today the transmission of signals using laser diodes and fibres has become an indispensable technology and the on-going development in this area is one of the most important within this century.

Following the achievements of communication technology, the development of fibre optical sensors began in 1977. Here the laser gyroscope for navigation has to be emphasised in particular. This new technology is based on well known fundamentals in a way that no new understanding has to be created. Still, there is a challenge with respect to the technical realisation, keeping in mind that the light has to be guided within fibres of only $5 \mu\text{m}$ diameter.

Appropriate fibres had to be developed and mechanical components of high precision had to be developed for coupling the light to the conductor (fibre) and for the installation of the fibres. Further goals are the reduction of transmission losses, optical amplification within the fibre as a replacement of the electronic amplifiers and laser diodes of small band width to increase the transmission speed of signals.

There is hardly any book in optics which does not contain the experiment of Colladan (1861) on total reflection of light. Most of us may have enjoyed it during the basic physics course.

An intensive light beam is introduced into the axis of an outflowing water jet. Because of repeated total reflections the light can not leave the jet and it is forced to follow the water jet. It is expected that the jet remains completely dark unless the surface contains small disturbances.

This leads to a certain loss of light and it appears illuminated all along its path. Effects of light created in this way are also known as “Fontaines lumineuses”. They generally please the onlookers of water fountains. This historical experiment already shows the physical phenomena which are basic in fibre optics. If we designate the diameter of a light guide with d we can state:

- ”Fontaines lumineuses”: $d \gg \lambda$
- Multimode fibre: $d > \lambda$

- Monomode fibre: $d = \lambda$

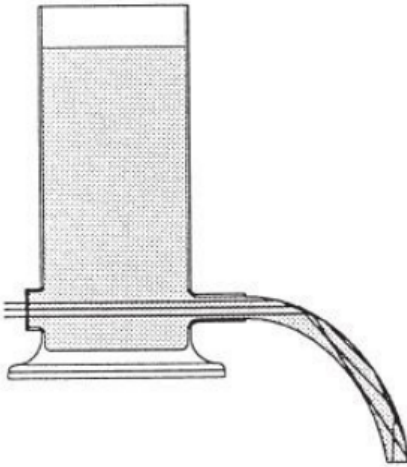


Figure 20: Colladan's (1861) experiment for the demonstration of the total reflection of light.

For the fibres manufactured these days, this leads to further effects which can not be described exclusively by total reflection. Their understanding is of special importance for optical communication technology. In the manual, we deduce these effects based on Maxwell's equations. For the work in fibre optics it is not compulsory to know this formalism. It is sufficient to familiarise oneself with the results. Nevertheless a few remarks are to be made with regard to the analytical formalism.

Within the frame of further considerations we will refer to fibres as light conductors which are made of glass or similar matter. They have no electric conductivity, no free charge carriers and no magnetic dipoles. Therefore the Maxwell equations adapted to our problem are as follows:

$$\begin{aligned}\nabla \times \vec{H} &= \epsilon \cdot \epsilon_0 \cdot \frac{\delta \vec{E}}{dt} \text{ and } \nabla \times \vec{H} = 0 \\ \nabla \times \vec{E} &= \frac{\delta \vec{H}}{dt} \text{ and } \nabla \times \vec{E} = 0\end{aligned}$$

ϵ_0 is the dielectric constant of the free space. It represents the ratio of the unit charge (As) to unit field strength (V/m) and amounts to $8.85910 - 12 \text{ As/Vm}$. ϵ is the dielectric constant of matter. It characterises the degree of extension of an electric dipole acted on by an external electric field E . The dielectric constant ϵ and the susceptibility χ are linked by the following relation:

$$\begin{aligned}\epsilon &= \frac{1}{\epsilon_0} \cdot (\chi + \epsilon_0) \\ \epsilon \cdot \epsilon_0 \cdot \vec{R} &= \vec{D}\end{aligned}$$

is therefore called "dielectric displacement" or displacement. ϵ_0 is the absolute permeability of the free space. It gives the context between the unit of an induced voltage (V) due to the presence of a magnetic field H of unit Am/s. It amounts to $1.256 \cdot 10^{-6} \text{ Vs/Am}$.

Using the above equations, the goal of the following calculations will be to get an appropriate set of equations describing the propagation of light in glass or similar matter. After this step

we will introduce the boundary conditions which have to be implemented due to the use of fibre glass with cladding. For details please refer to the manual.

Glass fibres as wave conductors have a circular cross section. They consist of a core of refractive index n_k . The core is surrounded by a glass cladding of refractive index n_m slightly lower than n_k . Generally the refractive index of the core as well as the refractive index of the cladding are considered homogeneously distributed. The boundary is between core and cladding. The final direction of the beam is defined by the angle Θ_e under which the beam enters the fibre. Unintended but not always avoidable radiation and cladding waves are generated in this way. For reasons of mechanical protection and absorption of the radiation waves, the fibre is surrounded by a protective layer.

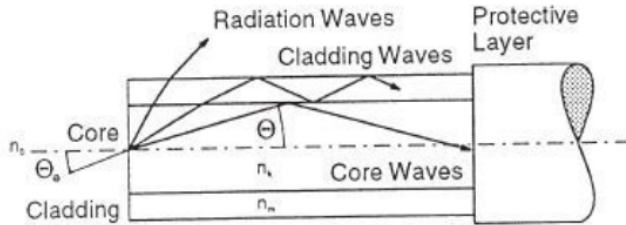


Figure 21: Step index fibre.

Figure reveals some basic facts which can be seen without having solved Maxwell's equations. Starting from geometrical considerations we can state that there must be a limiting angle Θ_c for total reflection at the boundary between cladding and core.

$$\cos \theta_c = \frac{n_m}{n_k}$$

For the angle of incidence of the fibre we use the law of refraction:

$$\frac{\sin \Theta_{cc}}{\sin \Theta_c} = \frac{n_k}{n_0}$$

and obtain:

$$\Theta_{ec} = \arcsin \left(\frac{n_k}{n_0} \cdot \sin \Theta_c \right)$$

Using the above equation and with $n_0 = 1$ for air we finally get:

$$\Theta_{ec} = \arcsin \left(\sqrt{n_k^2 - n_m^2} \right)$$

The limiting angle Θ_{ec} represents half the opening angle of a cone. All beams entering this cone will be guided into core by total reflection. As usual in optics here, too, we can define a numerical aperture A :

$$A = \sin \Theta_{ec} = \left(\sqrt{n_k^2 - n_m^2} \right)$$

Depending under which angle the beams enter the cylindrical core through the cone they propagate in a screw. This becomes evident if we project the beam displacements onto the XY-plane

of the fibre. The direction along the fibre is considered as the direction of the z-axis. A periodical pattern is recognised. It can be interpreted as standing waves in the XY-plane. In this context the standing waves are called oscillating modes or simply modes. Since these modes are built up in the XY-plane, e. g. perpendicularly to the z-axis, they are also called transverse modes. Modes built up along the z-axis are called longitudinal modes.

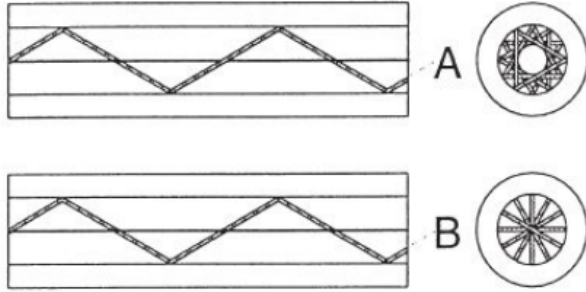


Figure 22: Helix (A) and Meridional beam (B).

The Bessel function is a suitable solution for the core. For the classing we need, in addition, an attenuation of the field. Here the modified Hankel function offers a promising solution. For $x \rightarrow 0$ and $r \rightarrow 0$ it turns to infinity but we only need it for the range $r \leq a$ (cladding).

For the ranger $r \geq a$ (core) we shall use the Bessel function. For solving the problems at the boundary between core and cladding we shall use the continuity conditions of the components of E and H for the transition from core to cladding and fit the Bessel and Hankel function for $r = a$.

Figure 23 presents one solution in the core. We now see how the electric field will establish within the core. It also becomes clear that the radius of the fibre will be decisive for the order of the modes. In the radial direction of the fibre we observe a main maximum at $r = 0$ and, further aside, maxima or minima which are also called nodes. The number of nodes is determined by the diameter of the fibre as well as by the solution of the wave equation within the cladding.

After having chosen a suitable cylindrical function for the solution within the cladding, it has to be ensured that it matches the continuity conditions for the electric and magnetic field at the boundary between core and cladding. This leads to the complete solution.

For the waves within the cladding, $r \geq a$, we want to achieve that the radial field of the core rapidly decreases in the cladding to favour the guidance of waves within the core. If the fibre is made in a way that only the fundamental wave is guided within the core the fibre is called a monomode or singlemode fibre. In all other cases we speak about a multimode fibre. Depending on the range of application of the fibre one uses one or the other type of fibre. Let's now derive the "construction"-rule for a fibre from the solutions allowing us to define the conditions under which a fibre "accepts" an incoming wave at given wavelength and guides it as a monomode fibre.

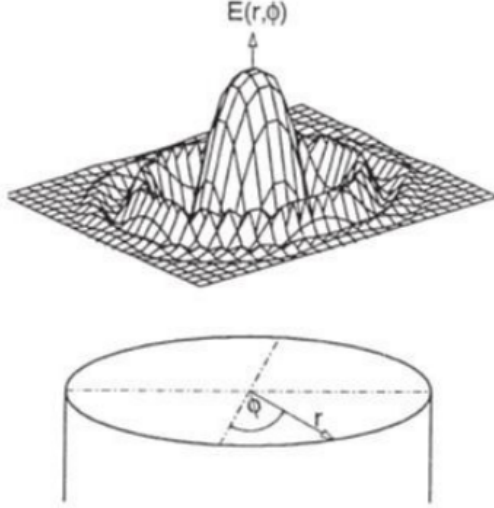


Figure 23: Solution of Bessel function in the core.

The condition for the transmission of the fundamental wave exclusively is (see manual):

$$0 < \frac{2\pi}{\lambda} a \sqrt{n_k^2 - n_m^2} \leq 2.405$$

The above equation represents an important prescription for the design of the fibre. It fixes the radius a of the core for monomode waveguidance if the wavelength λ and the refractive index for cladding and core have been selected.

If, for example, the problem would be to transmit the light of a Helium-Neon laser (wavelength 633 nm, refractive index of cladding 1.4) we would get the following range for the radius a :

$$a < 2.405 \cdot \frac{633 \cdot 10^{-9}}{2\pi\sqrt{(1.5)^2 - (1.4)^2}} = 0.45 \mu m$$

The result depends strongly on the difference of the refractive index. The smaller this difference the greater can be the radius a . Still, because of technical reasons it is not possible to choose the refractive index of the core much larger than the refractive index of the cladding. Since core and cladding are in close contact glasses of similar temperature coefficient can only be used. The consequence of this is the small difference in refractive index.

For ordinary fibres it is

$$\frac{n_k - n_m}{n_k} = 2 \cdot 10^{-3}$$

where the refractive index n_k of the core is equal to 1.465. If we use these values for the above mentioned example we get:

$$0 < a < 2.405 \cdot \frac{633 \cdot 10^{-9}}{2\pi\sqrt{(1.5)^2 - (1.4)^2}} = 0.45 \mu m$$

The diameter of the fibre should be chosen smaller than $5.2 \mu m$ to get the desired monomode transmission. We are facing the problem to couple a beam of light to a fibre, respectively to introduce it into fibre, the diameter of which is in the order of magnitude of 4-10 μm and in so

far comparable to the wavelength of light.

To get a sufficient high excitation of the fundamental mode of the fibre, the beam of the light source has to be focused to a diameter of this order of magnitude. Under these circumstances the laws of geometrical optics fail because they anticipate parallel light beams or plane light waves which in reality exist only in approximation.

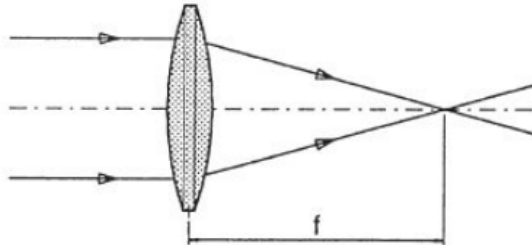


Figure 24: Focusing two beams in geometrical optics.

Real parallel light beams do not exist in reality and plane wave fronts exist only at a particular point. The reason for the failure of geometrical optics is the fact that it has been defined at a time where the wave character of light was still unknown as the possibility to describe its behaviour by Maxwell's equations.

To describe the propagation of light we use the wave equation

$$\Delta \vec{E} - \frac{n^2}{c^2} \cdot \frac{\delta \vec{E}}{\delta t^2} = 0$$

Solving this equation for the fibre we anticipated waves propagating within the fibre as a cylindrical body

$$\vec{E} = \vec{E}(r, \theta, z) \text{ with } r^2 = x^2 + y^2$$

Without a boundary, light would propagate as a spherical wave in all directions of the space.

$$\vec{E} = \vec{E}(r) \text{ with } r^2 = x^2 + y^2 + z^2$$

When we consider the technically most important case of spherical waves propagating in the direction of z within a small solid angle, we arrive at the following statement for the electrical field:

$$\vec{E} = \vec{E}(r, z) \text{ with } r^2 = x^2 + y^2$$

In this case the solution of the wave equation provides fields which have a Gaussian intensity distribution over the cross-section. Therefore they are called Gaussian beams. Similar to the solutions of the fibre the Gaussian beams exist in different modes depending on the actual boundary conditions.

Such beams, especially the Gaussian fundamental mode (TEM_{00}) are generated with preference by lasers. But the light of any light source can be considered as the superposition of many such Gaussian modes. Still, the intensity of a particular mode is small with respect to the total

intensity of the light source.

The situation is different for the laser. Here the total light power can be concentrated in the fundamental mode. This is the most outstanding difference with respect to ordinary light sources next to the monochromasy of laser radiation. Gaussian beams behave differently from geometrical beams.

A Gaussian beam always has a waist. The beam radius ω results out of the wave equation as follows:

$$\omega(z) = \omega_0 \cdot \sqrt{1 + \left(\frac{z}{z_r}\right)^2}$$

ω_0 is the smallest beam radius at the waist and z_r is the Rayleigh length

$$z_r = \omega_0^2 \frac{\pi}{\lambda}$$

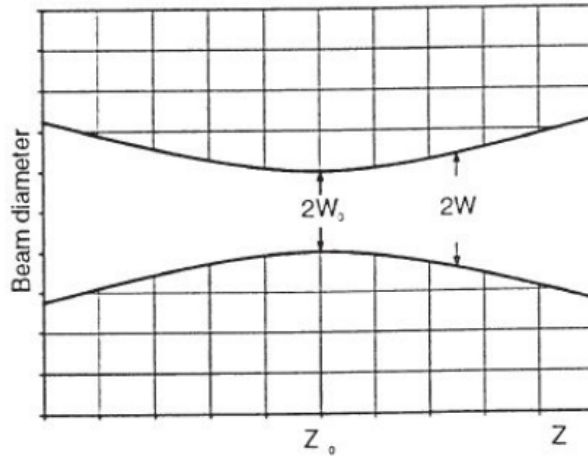


Figure 25: Beam diameter of a Gaussian beam as fundamental mode TEM00 and function of z .

In the figure, the course of the beam diameter as a function of z is represented. The beam propagates within the direction of z . At the position $z = z_0$, the beam has the smallest radius. The beam radius increases linearly with increasing distance.

Since Gaussian beams are spherical waves we can attribute a radius of curvature of the wave field to each point z . The radius of curvature R can be calculated using the following relation:

$$R(z) = z + \frac{z_r^2}{z}$$

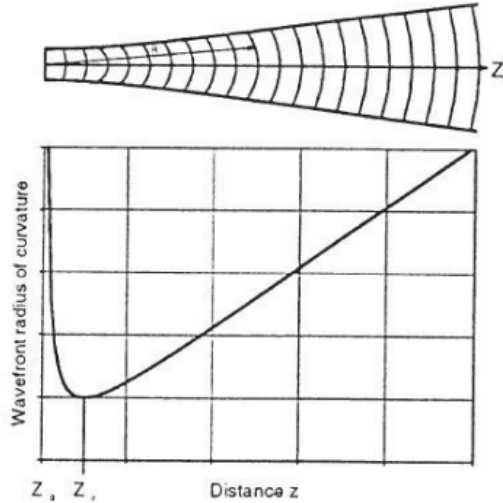


Figure 26: Course of the radius of curvature of the wavefront as a function of the distance from the waist at $z = 0$.

This context is reflected by this figure. At $z = z_r$, the radius of curvature has a minimum. Then R increases with $1/z$ if z tends to $z = 0$. For $z = 0$ the radius of curvature is infinite. Here the wavefront is plane. Above the Rayleigh length z_r , the radius of curvature increases linearly. This is a very essential statement. Due to this statement a parallel beam only exists at one point of the light wave, to be precise only in its focus. Within the range

$$-z_r \leq z \leq z_r$$

a beam can be considered as parallel or collimated in good approximation.

In this figure, the Rayleigh range has been marked as well as the divergence θ in the farfield, that means for $z \gg z_0$. The graphical representations do not well inform you about the extremely small divergence of laser beams which is another outstanding property of lasers.

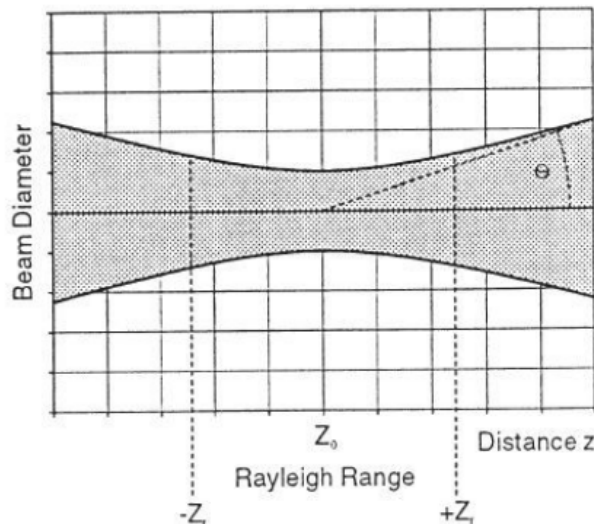


Figure 27: Rayleigh range z_r and divergence θ for the farfield $z \gg z_r$.

The reason for this is that the ratio of the beam diameter with regard to z has not been normalised. Let's consider, for example, a He-Ne laser (632 nm) with a beam radius of $\omega_0 = 1$ mm at the exit of the laser. For the Rayleigh range $2z_r$ we get:

$$2z_r = 2\omega_0^2 \frac{\pi}{\lambda} = 2 \cdot 10^{-6} \frac{3.124}{6.23 \cdot 10^{-9}} = 9.9 \text{ m}$$

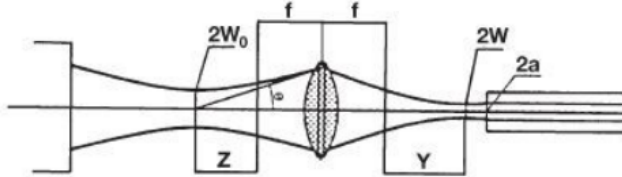


Figure 28: For the calculation of the coupling optic.

To get a maximum of power into the fibre a coupling optic of focal distance f is required assuring the coupling of a Gaussian beam into a weak guiding step index fibre in the fundamental mode.

The radius at the waist is

$$\omega = \frac{\omega_0 \cdot f \cdot \theta}{\sqrt{\omega_0^2 + \theta^2 \cdot z^2}}$$

The position of the waist is

$$y = \frac{z \cdot f^2}{z^2 + \left(\frac{\omega_0}{\theta}\right)^2}$$

Example: The beam of a He-Ne laser of 0.5 mm diameter and of 1.5mrad divergence is made to focus by means of a lens. The focal distance is 50 mm and the lens is at a distance of 2 m from the laser. We find:

$$\begin{aligned} \omega &= \frac{0.5 \cdot 10^{-3} \cdot 0.05 \cdot 1.5 \cdot 10^{-3}}{\sqrt{0.25 \cdot 10^{-6} + 2.25 \cdot 10^{-6} \cdot (2 - 0.05)^2}} = 12.6 \mu\text{m} \\ y &= \frac{(2 - 0.05) \cdot 2.5 \cdot 10^{-6}}{(2 - 0.05)^2 + \left(\frac{0.5}{1.5}\right)^2} = 1.25 \mu\text{m} \end{aligned}$$

For this example the position y of the waist coincides with the focus in good approximation and the radius of the waist is here $12.6 \mu\text{m}$. To get the fibre under consideration adapted in an optimal way, the focal distance f has to be chosen in a way that the radius of the beam is equal to the radius of the core. When laser diodes are used, the preparation of the beam becomes more complicated.

3.4 Results and Discussion

Task 1

Following the outlined procedure, we assembled the experiment using the provided kit. The figure below illustrates the outcome of our initial setup.

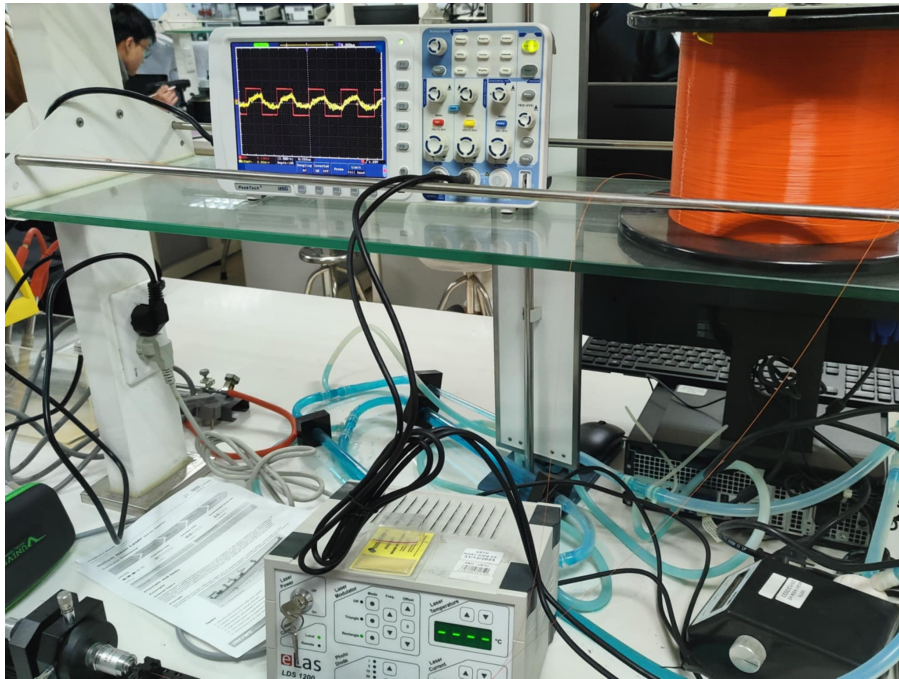


Figure 29: Set-up and output signal

Task 2

Figures below presents the images captured during our measurements of the relative output power. Each image corresponds to a measurement taken at a different angle readout.

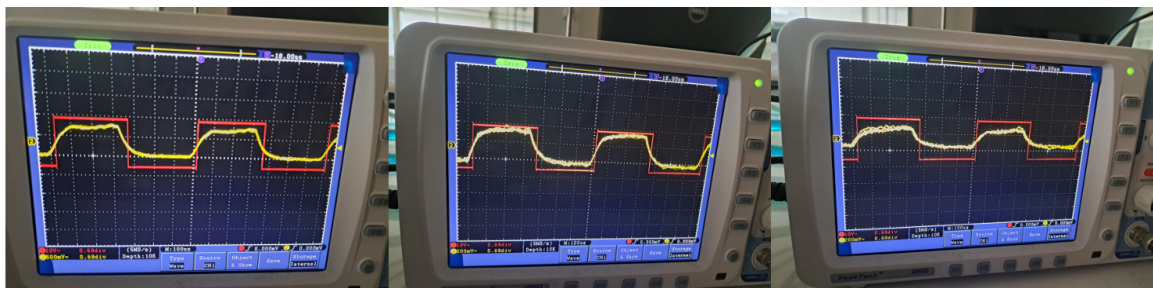


Figure 30: Measurements of relative output power with changing angle readout

Task 3

Figures below displays the images captured during our measurements of the relative output power of the diode laser. Each image represents a measurement taken at a different injection current.



Figure 31: Measurements of relative output power of diodelaser with changing injection current

Injection current (mA)	10	20	30	40	50	60	70
Output power	0	0	0.01	0.025	0.05	0.2	0.45

Table 10: Relative output power vs injection current

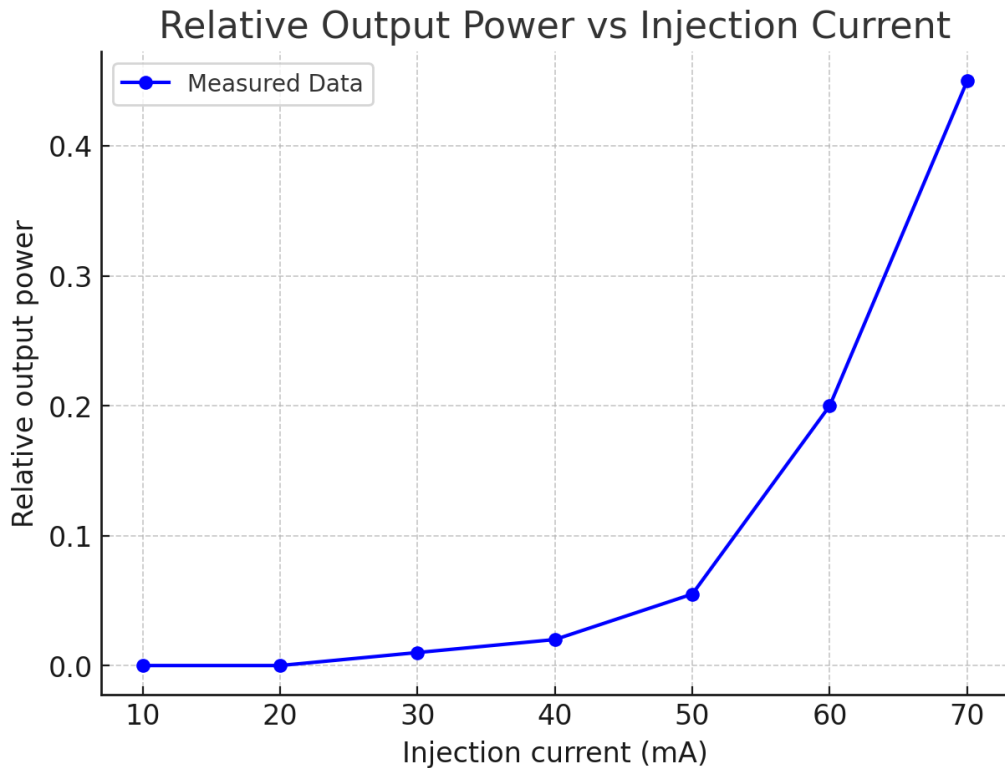


Figure 32: Relative output power of the diode laser versus injection current

Figure presents the results of the measurements. It clearly indicates the presence of a threshold current required to generate laser radiation. Once this threshold is surpassed, the output power exhibits a linear increase with the supply current.

4 Measuring the velocity of light

4.1 Overview

Application

Although light travels very fast, its velocity is finite. Since 1676, when Romer estimated the velocity of light using spatial scales that included the distances to the moons of Jupiter, much technical development took place.

In astronomy, the velocity of light has been used to measure the distances in the solar system. For example, it takes light 8 minutes and 17 seconds to travel from the Earth to the Sun, which the distance can be defined as 149,597,870 km.

Prior knowledge

Light is an oscillating electromagnetic wave that could travel from one medium to another medium. If it reaches the interface between the two media, some part of the incident beam is reflected and some is transmitted, which known as refraction.

Scientific principle

The intensity of a laser diode is modulated with a high frequency and the beam is reflected, after travelling some distance, back into the apparatus. The phase of the received signal is compared to the one transmitted. The velocity of light is then calculated from the measured phase difference, the modulation frequency and the length of the light path.

Objective

To study the influences of refractive index on the velocity of light, by allowing the laser beam to propagate in transparent media, e.g. air, glass and water.

Equipment

Position	Material	Item No.	Quantity
1	Speed of Light Meter Set	11226-88	1
2	Screened cable, BNC, l = 750 mm	07542-11	2
3	Digital storage oscilloscope, 20 MHz, 2 channels, 100 MS/s	EAK-P-1335	1

Table 11: Equipment for labwork 04.

Task

1. Determine the velocity of light in air.
2. Determine the velocity of light in water and calculate the refractive index.
3. Determine the velocity of light in acrylic glass and calculate the refractive index.

4.2 Setup and Procedure



Figure 33: Setup for labwork 04.

The experiment set-up is shown in the Figure 33. The light velocity measuring apparatus and the mirror are set up in such a way that the laser beam hits the mirror no matter where along the base the mirror is placed (more detailed directions can be found in the operating instructions of the Speed of Light meter).

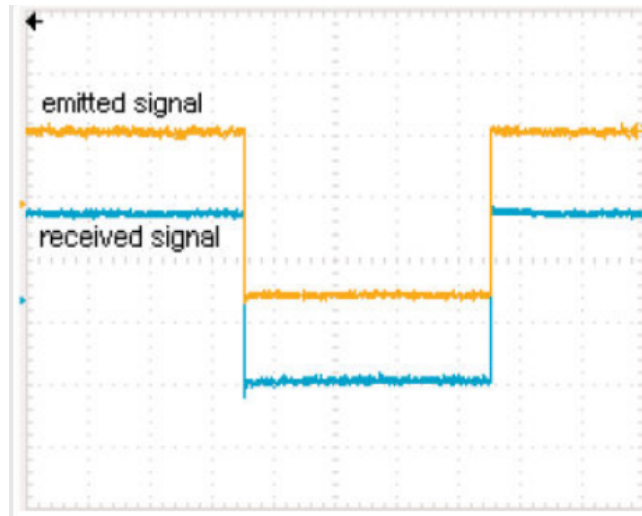


Figure 34: Oscilloscope signal after "Calibration".

The socket ($\frac{f_{\text{emit}}}{1000}$) is connected to the oscilloscope and the modulation frequency f_{emit} (divided by 1000) is determined.

The two other sockets ($f_{\text{emit}} - f_{\text{sync}}$) and ($f_{\text{rec}} - f_{\text{sync}}$) are connected to the two input sockets of the oscilloscope. The frequencies of the emitted and the received signal are also reduced to 50 kHz while conserving their phase relation so that they can be displayed on this type of oscilloscope.

The "Calibration" button is pressed for every new measurement.

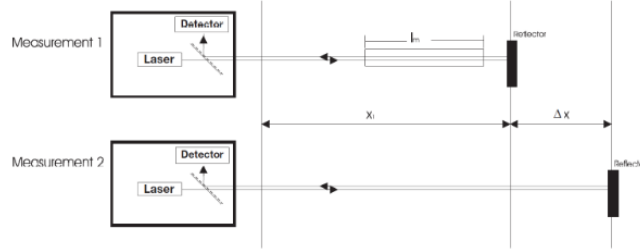


Figure 35: Oscilloscope signal after "Calibration".

Task 1: The velocity of light in air

At the start the mirror is placed close to the operating unit, the mode " $\Delta\varphi$ " is selected and the button "Calibration" is pressed to have two coinciding signals visible on the oscilloscope.

The mirror is then slid along the graduated scale. For at least 10 different displacements $\Delta x > 1000$ mm the time difference Δt is calculated from the readings performed on the oscilloscope.

Task 2+3: The velocity of light in water and in acrylic glass

The water-filled tube or the acrylic glass rod is placed so that the laser beam runs through them, the mirror is placed directly behind. The rod is then taken out of the path of the rays, the two signals will not coincide any longer.

Now the mirror is moved a distance Δx until the two signals on the oscilloscope coincide again as before with the medium inserted. The mirror displacement Δx is measured several times.

4.3 Theory and Evaluation

In the SI system, the metre is defined as the distance light travels in vacuum in $1/299\ 792\ 458$ of a second. The effect of this definition is to fix the speed of light in vacuum at exactly $299\ 792\ 458$ m/s and it is denoted by c . To obtain the speed of light, one has to calculate $\Delta s/\Delta t$, where Δt is the time which the light takes to travel the distance Δs .

During the propagation of light in other medium, such as glass or water, the light travels slower than in vacuum. The ratio between c and the speed v at which the light travels in a medium is called the refractive index n of the medium ($n = c/v$). Increasing refractive index corresponds to decreasing speed of light in the medium. When light leaves the medium and returns to a vacuum, its velocity returns to the usual speed of light.

Velocity of light in air

To obtain the velocity of light, one must calculate $\frac{\Delta s}{\Delta t}$. The distance Δs is $2 \cdot \Delta x$ because the additional stretch is twice the mirror displacement since the laser beam has to travel to the

mirror and back again.

Velocity of light in water/acrylic glass

The velocity of light in water or acrylic glass, v_m , is measured by comparing it with the velocity of light in air c . In the first measurement (with the medium), the light travels a distance l_1 in time t_1 ($l_1 = 2\Delta x$).

In the second measurement (no medium), the light travels a distance $l_2 = l_1 + 2\Delta x$ in the same time. This means that light takes the same time to travel the distance $2\Delta x + 2l_m$ in air as it takes to travel the distance $2l_m$ in the medium.

From this and the definition of the refractive index, it follows directly that:

$$n_m = \frac{(2\Delta x + 2l_m)}{2l_m} = \frac{(\Delta x + l_m)}{l_m}$$

4.4 Results and Discussion

Task 1



Figure 36: Practical set-up of experiment with provided equipment

Δx in min	Δs in mm	Δt in s	c in m/s . e8
1000	2000	7e-6	2.86
1100	2200	7.67e-6	2.87
1200	2400	8.50 e-6	2.82
1300	2600	9.28e-6	2.80
1350	2700	9.78e-06	2.76
1400	2800	1.02e-05	2.75
1450	2900	1.07e-05	2.70
1500	3000	1.13e-05	2.66
1550	3100	1.19e-05	2.61
1600	3200	1.21e-05	2.64

Table 12: Velocity of light in air

The average value of velocity of light is 2.75e8 which is 91.67 % of the actual speed of light. The error might due to human error, technical error and the medium is not completely homogeneous.

Task 2

l_m in mm	Δx in mm	n_m	c in m/s . e8
50	34	1.68	1.64
55	29	1.527	1.8
60	27	1.45	1.9
70	30	1.429	1.92

Table 13: Velocity of light in acrylic glass

The average velocity of light is 1.81e8 which is 60.5 % speed of light. And the average value of acrylic glass index is 1.521. The measured refractive index of acrylic glass (1.521) deviates from the accepted value (1.49) by approximately 2.08 %. This discrepancy suggests systematic or experimental errors in the measurement process, though the result is reasonable for educational settings given potential limitations in equipment or methodology.

Task 3

l_m in mm	Δx in mm	n_m	c in m/s . e8
60	25.7	1.428	2.1
70	25.6	1.368	2.2
120	25	1.208	2.5

Table 14: Velocity of light in water

The average value of the refractive index is 1.3333 which is the correct value for water. If we continue make experiment, we can get closer to the right value.

5 Fresnel's law

5.1 Overview

Principle

Plane-polarized light is reflected at a glass surface. Both the rotation of the plane of polarization and the intensity of the reflected light are to be determined and compared with Fresnel's formulae for reflection.

Equipment

Laser, He-Ne 1.0 mW, 220 V AC	08181.93	1
Polarising filter, on stem	08610.00	2
Prism, 60 degrees, h 36.4 mm, flint	08237.00	1
Prism table with holder	08254.00	1
Photoelement f. opt. base plt.	08734.00	1
Protractor scale with pointer	08218.00	1
Articulated radial holder	02053.01	1
Stand tube	02060.00	1
Tripod base -PASS-	08734.00	1
Photoelement f. opt. base plt.	02002.55	1
H-base -PASS-	02009.55	1
Right angle clamp -PASS-	02040.55	1
Support rod -PASS-, square, l 400 mm	02026.55	1
Support rod -PASS-, square, l 250 mm	02025.55	1
Support rod -PASS-, square, l 630 mm	02027.55	1
Multirange meter with amplifier	07034.00	1
Dry cell, 1.5 V	11620.34	6

Table 15: Equipment for labwork 05.

Task

1. The reflection coefficient of light, which is polarised either perpendicularly or parallel to the plane of incidence, is to be determined as a function of the angle of incidence and plotted graphically.
2. The refraction index of the flint glass prism is to be determined.
3. The refraction coefficient is to be calculated by means of Fresnel's formula and compared to the measured curve.
4. The reflection factor for flint glass is calculated.
5. The rotation of the plane of polarisation for linearly polarised light after reflection is determined as a function of the angle of incidence and plotted graphically. This is compared to the values calculated by means of Fresnel's formula.

5.2 Setup and Procedure



Figure 37: Practical set-up for the determination of the rotation of the plane of polarization by reflection

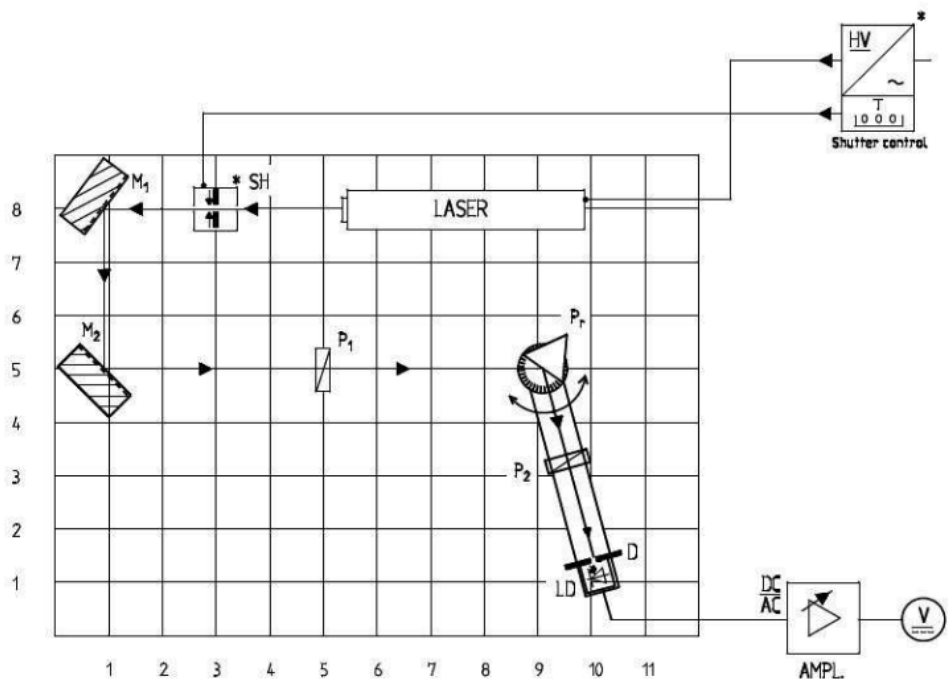


Figure 38: Experimental set up for the verification of the rotation of the plane of polarisation due to reflection (* only required for 5 mW laser).

The experimental set up is shown in Fig. 38. The recommended set up height (height of beam path) should be 130 mm.

Set up of the rotating unit

To start with, the stopping screw of a magnet foot is removed. The circular orifice of the rotating guide rail is set under the foot. The angular scale is set onto the magnet foot and also on top of the rotating guide rail. The magnet foot is fixed to the optical base plate, and the rotating guide rail can be shifted sufficiently. Photocell LD can be fixed to one end and polarisation filter P_2 to the middle of the rotating guide rail, both by means of a magnet foot. During the set up of the optical base plate, the angular distribution should be reasonable, that is, the 0° scale mark should be directed towards the incident laser beam.

Prism Pr should be placed with the forward surface edge exactly on the central point of the table. The laser beam is then adjusted onto the central axis of the prism and of the table by means of adjusting screws M_1 and M_2 .

Concerning measurement

After letting the laser warm up for about 15 minutes, experimental set up is carried out without polarisation filter P_2 to start with.

To determine the incident intensity I_0'' of the light polarised parallel to the plane of incidence (pointer of polarizer P_1 set to 90°), the prism is removed and the rotating guide rail is rotated so that the laser beam falls directly onto the photocell (amplification of the universal measurement amplifier must be adjusted in such a way that voltage does not increase above the maximum output voltage of 10 V).

After the prism has been replaced onto the prism table, the rotating guide rail with detector LD is set to an angle φ of about 10° . The prism table carrying the prism is now turned so that the reflected beam is directed towards detector LD. According to Snellius's law, the angle of incidence is equal to the exiting angle, that is, angle of incidence α is half the angle φ formed by the incident laser beam and the rotating guide rail.

The angle of the rotating guide rail is now modified in steps of 5° (steps of about 2.5° in the area of Brewster's angle). The prism is turned every time in such a way that the laser beam falls on the detector, in order to determine light intensity I_0'' . Angle φ should be varied up to about 160° .

This experiment is repeated with light polarised perpendicularly to the plane of incidence of the prism (pointer of polarizer P_1 set to 0°). For this, the intensity of the incident laser beam without prism, I_0^1 , must be determined to start with.

Concerning the second part of measurements

Polarising filter P_2 is brought into the beam path between prism and photocell on the rotating guide rail. Polarizer P_1 is set to an angle of 45° (pointer set to 45°). Without prism, detector LD would indicate an intensity minimum if the polarising directions of the two polarising filters P_1 and P_2 were crossed (P_2 pointer at -45°). One makes use of the fact that the intensity minimum

can be determined more precisely than the peak, so that during reflection at the prism, one looks for the intensity minimum through rotation of polarising filter P_2 . The rotation supplementary to -45° is the rotation of the plane of polarisation Ψ due to reflection at the prism. This is carried out for different angles of incidence α of the laser beam on the surface of the prism. Variation of the angle of incidence is carried out as in the first part.

5.3 Theory and Evaluation

In a light wave, the electric field vector E and the magnetic vector B oscillate perpendicularly and in phase to each other.

Intensity is given by Maxwell's equation:

$$|B| = n \cdot |E| \quad (43)$$

where n is the refraction index of the medium through which the light beam travels. The energy of the wave transported in the direction of propagation is given by Poynting's vector, according to the following relation:

$$S \approx E \times B \quad \text{and} \quad |S| \approx |E|^2 \quad (44)$$

If light falls onto a boundary surface of an isotropic medium of refraction index n with an angle of incidence α , part of the intensity is reflected and the rest goes through the medium under an angle of refraction β . The following indexes are used in the theory mentioned below:

x^\perp, x'' direction of oscillation of the electric and magnetic field vectors, which are directed either parallel

x_0, x_r, x_t Incident, reflected and refracted vector components.

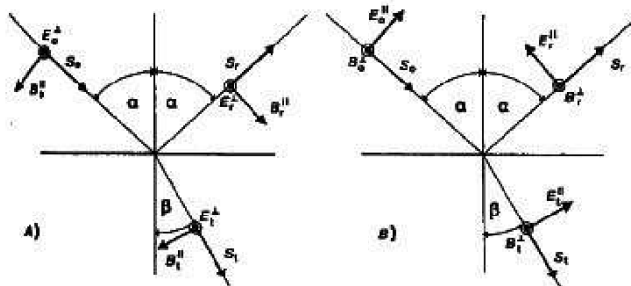


Figure 39: A) direction of oscillation of the electric field vector perpendicularly and B) parallel to the direction of incidence.

In Fig. 39, the electric field vector E_0 of the incident light wave oscillates perpendicularly to the plane of incidence. Magnetic vector B_0'' oscillates parallel to the latter. Related to the law of continuity of the tangential components (that is, the components which oscillate parallel to the surface of the object) and to the direction of the beam, the following relation holds:

$$\begin{aligned} E_0^\perp + E_r^\perp &= E_t^\perp \\ (B_0'' - B_r'') \cos \alpha &= B_t'' \cos \beta \end{aligned}$$

We obtain:

$$(E_0^\perp - E_r^\perp) \cos \alpha = n(E_0^\perp + E_r^\perp) \cos \beta$$

Taking into account the law of refraction, the relation of field intensities is:

$$\zeta^\perp = \frac{E_r^\perp}{E_0^\perp} = \frac{\cos \alpha - n \cos \beta}{\cos \alpha + n \cos \beta}$$

where ζ^\perp is defined as the reflection coefficient.

Fig. 39 shows an incident light wave, whose vector E''_0 oscillates perpendicularly to the plane of incidence. The following is obtained:

$$\begin{aligned} B_0^\perp + B_r^\perp &= B_t^\perp \\ E''_0 - E''_r \cos \alpha &= E''_t \cos \beta \\ (E''_0 - E''_r) \cos \alpha &= \frac{1}{n} (E''_0 + E''_r) \cos \beta \end{aligned}$$

Fresnel's formulae and can be written in a different form, eliminating refraction angle β by means of Snellius' law of refraction:

$$\begin{aligned} \zeta^\perp &= \frac{E_r^\perp}{E_0^\perp} = - \left(\frac{\sqrt{n^2 - \sin^2 \alpha} - \cos \alpha}{n^2 - 1} \right) \\ \zeta'' &= \frac{E''_r}{E''_0} = \frac{n^2 \cos \alpha - \sqrt{n^2 - \sin^2 \alpha}}{n^2 \cos \alpha + \sqrt{n^2 - \sin^2 \alpha}} \end{aligned}$$

$\zeta^\perp \geq \zeta''$ is valid for all angles of incidence α between zero and $\frac{\pi}{2}$

Special cases

A: The following relation is valid for perpendicular incidence ($\alpha = \beta = 0$):

$$\zeta^\perp = \zeta'' = \frac{n - 1}{n + 1}$$

B: For a grazing angle ($\alpha = \frac{\pi}{2}$), the following holds:

$$\zeta^\perp = \zeta'' = 1$$

C: If the reflected and the refracted beams are perpendicular to each other ($\alpha + \beta = \frac{\pi}{2}$).

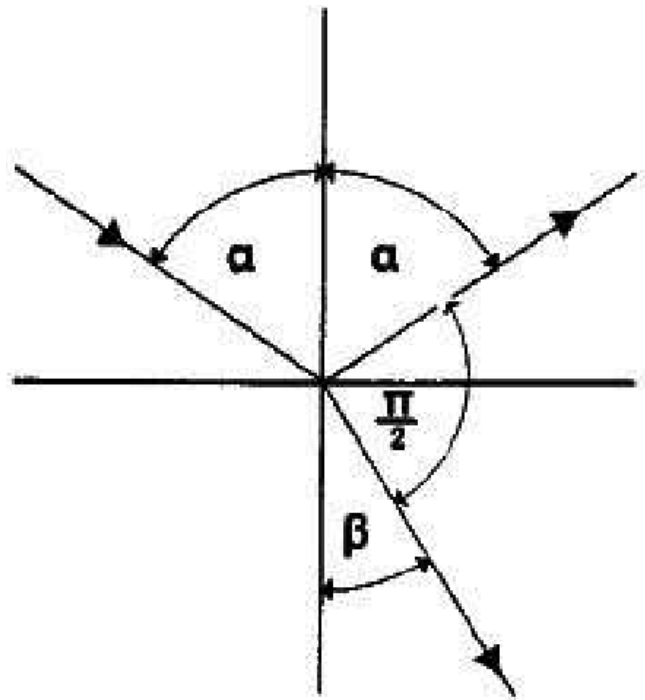


Figure 40: Brewster's law.

As shown in Fig. 40, there follows:

$$\zeta'' = 0$$

that is, reflected light is completely polarised. In this case, the electric vector oscillates only perpendicularly to the plane of incidence. Related to Snellius' law of refraction, the following is valid:

$$\sin \alpha = n \cdot \sin \beta = n \cdot \sin \left(\frac{\pi}{2} - \alpha \right) = n \cdot \cos \alpha$$

so that for this special case one obtains an angle of incidence from:

$$\tan \alpha_p = n$$

α_p = polarisation or Brewster's angle.

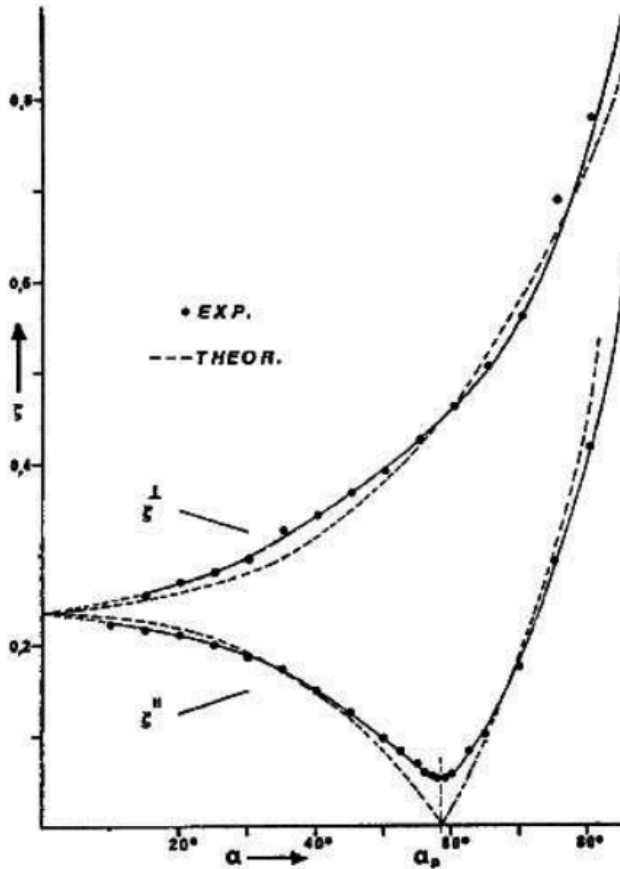


Figure 41: Measured and calculated curves for ζ''_r and ζ'_r as a function of the angle of incidence.

Fig. 41 shows the curves determined experimentally for ζ' and ζ'' as a function of the angle of incidence α . The curve for ζ' displays a significant minimum for $\alpha_p = 58.5^\circ$. With this value and the point of intersection of the ζ' curves with the ordinate axis, which can be obtained through extrapolation, applying (13) and (10), one obtains a value of $n = 1.63$ for the refraction index. The curve calculated theoretically according to (9), with $n = 1.63$, shows good agreement with experiment. The flatter curve of ζ'' at α_p is caused by the laser light which has a degree of polarisation < 1 . If the reflection components from (9a) and (9b) are squared and added, one obtains for the reflection factor R for perpendicular incidence:

$$R = \frac{(E_L^\perp)^2 + (E_R^\perp)^2}{(E_0)^2 + (E_0)^2} = \left(\frac{n-1}{n+1}\right)^2 \quad (45)$$

The reflection factor R for the flint glass prism ($n = 1.63$) is thus approximately 0.06.

Another possibility to verify Fresnel's formulae is based on the following method:

Linearly polarised light, with an electric field vector rotated by an azimuth angle δ against the plane of incidence, impinges on a glass reflector. The rotation of the plane of polarisation of the reflected beam is recorded as a function of the angle of incidence.

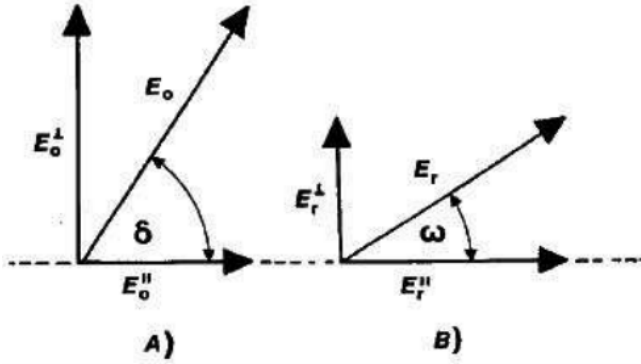


Figure 42: Rotation of the direction of oscillation through reflection.

In Fig. 42, the plane of the paper represents the reflection surface. If the electric vector oscillates under an angle ω after reflection, the rotation of the plane of polarisation is given by the angle $\Psi = \delta - \omega$. The following relation is true for the field components parallel and perpendicular to the plane of incidence:

$$E_r'' = E_r \cos \omega; \quad E_r = E_r \sin \omega$$

or

$$\tan \omega = \frac{E_r}{E_r''} = \frac{E_r^\perp}{E_r^\parallel} \cdot \frac{E_0^\perp}{E_r^\perp}$$

We obtain:

$$\tan \omega = - \left(\frac{\sin(\alpha - \beta)}{\sin(\alpha + \beta)} \right) \cdot \left(\frac{\tan(\alpha + \beta)}{\tan(\alpha - \beta)} \right) \cdot \tan \delta$$

For the special case with $\delta = \frac{\pi}{4}$, the following holds:

$$\tan \Psi = \tan \left(\frac{\pi}{4} - \omega \right) = \frac{1 - \tan \omega}{1 + \tan \omega}$$

We obtain:

$$\tan \Psi = \frac{\cos(\alpha + \beta) + \cos(\alpha - \beta)}{\cos(\alpha + \beta) - \cos(\alpha - \beta)} = - \left(\frac{\cos \alpha \sqrt{1 - \sin^2 \beta}}{\sin \alpha \sin \beta} \right)$$

The definitive formula is obtained through elimination of refraction angle β through the law of refraction:

$$\Psi = \arctan \left(- \left(\frac{\cos \alpha \sqrt{n^2 - \sin^2 \alpha}}{\sin^2 \alpha} \right) \right)$$

If the plane of polarisation is turned by $\Psi = \frac{\pi}{4}$, Brewster's law results:

$$\tan \alpha_p = n$$

Fig. 43 shows the measured rotation of the plane of polarisation as a function of the angle of incidence with good agreement with the values calculated by means of equation.

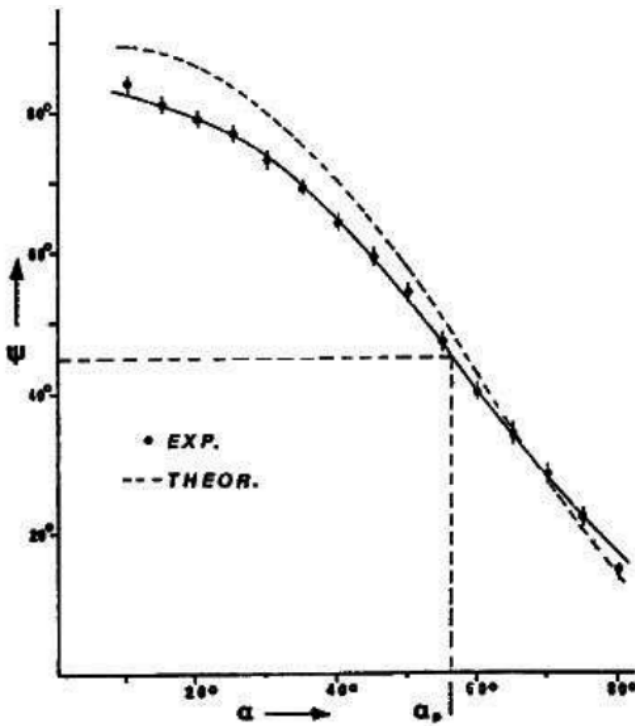


Figure 43: Measured and calculated curves for the rotation of the direction of oscillation as a function of the angle of incidence (the azimuth of the incident beam is 45°).

5.4 Results and Discussion

Task 1

The table below presents the measured values of the reflection coefficient corresponding to each angle of incidence.

Angle ($^\circ$)	0	15	30	45	60	75	90	105	120	135	150	165
ζ^{\parallel}	3.35	0.852	0.533	0.370	0.174	0.153	0.129	0.072	0.045	0.03	0.018	0.018
ζ^{\perp}	3.35	0.361	0.072	0	0.009	0	0.003	0	0.003	0.006	0.006	0.006

Table 16: Reflection coefficients for different angles of incidence

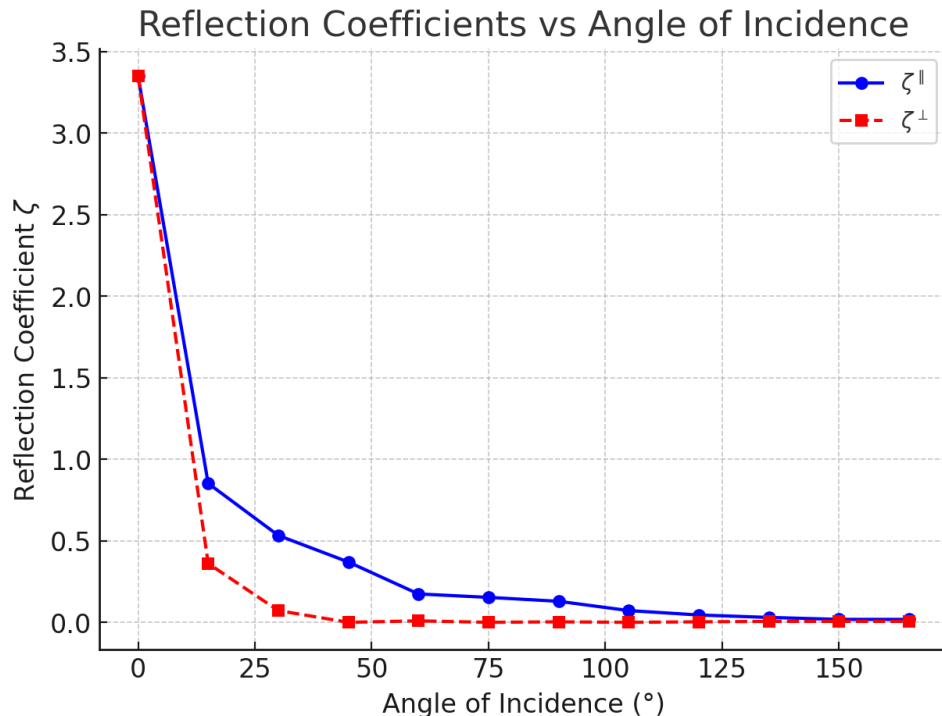


Figure 44: Reflection coefficients as a function of angle of incidence for light polarized perpendicular and parallel to the plane of incidence

Task 2

If the reflected and refracted beams are perpendicular to each other ($\alpha + \beta = \pi/2$), the perpendicular reflection coefficient is zero $\zeta^\perp = 0$. In this scenario, the reflected light beam becomes fully polarized, with its electric vector oscillating solely perpendicular to the plane of incidence. According to Snell's law of refraction:

$$\sin(\alpha) = n \sin(\beta) = n \sin(\pi/2 - \alpha) = n \cos(\alpha)$$

From 16, selecting an incident angle of $\alpha = 45^\circ$ where $\zeta^\parallel = 0$, we apply the equation above to determine the refractive index of the flint glass prism:

$$n = \frac{\sin(45^\circ)}{\cos(45^\circ)} = 1.61$$

Task 3

Using Fresnel's equations with a refractive index of $n = 1.61$, the theoretical reflection coefficients are presented in the table below.

Table 17: Reflection Coefficients from Theoretical Calculation

Angle (α)	ζ^{\parallel}	ζ^{\perp}
0°	0.234	0.234
15°	0.224	0.244
30°	0.190	0.277
45°	0.118	0.343
60°	-0.022	0.462
75°	-0.314	0.665
90°	-1	1
105°	-3.176	1.501
120°	-4.07	2.163
135°	8	2.907
150°	5.27	3.6
165°	4.462	4.090

Task 4

To calculate the reflection factor R , we can apply equation:

$$R = \left(\frac{n-1}{n+1} \right)^2 = \left(\frac{1.61-1}{1.61+1} \right)^2 = 0.054$$

Task 5

For calculating rotation of the polarization plane, we have the table below.

Angle (α)	ψ
0°	
15°	87.5
30°	79.4
45°	64.12
60°	42.39
75°	19.8
90°	0
105°	19.8
120°	42.39

Table 18: Measured and calculated curves for the rotation of the direction of oscillation

Figure below illustrates the measured rotation of the plane of polarization as a function of the angle of incidence, showing strong agreement with the theoretical values.

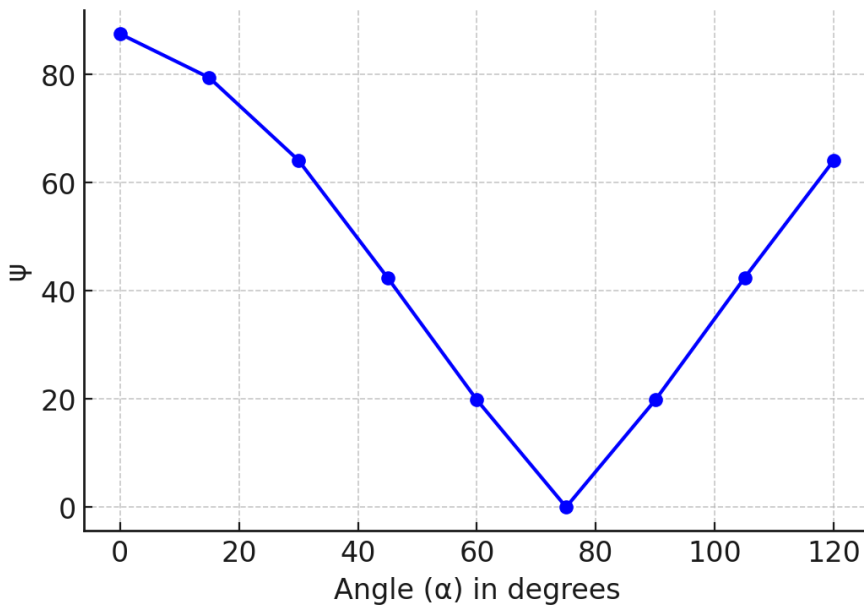


Figure 45: Calculated curves for the rotation of the direction of oscillation as function of the angle of incidence

6 Helium-Neon Laser

6.1 Overview

Safety instructions

- Never look directly into the laser beam!
- Avoid skin exposure to the laser beam!
- Wear suitable eye protection!
- Control the access to area of laser operation. Limit the access to this area to persons required to be there and those who have been instructed in the safe operation of lasers.
- Post warning signs in prominent locations near the laser area.
- Do not set up experiments at eye level.
- Provide enclosed paths for laser beams when possible.
- Keep the beam path as short as possible.
- Keep the number of changes of the direction of the beam as low as possible.
- The laser beam should not cross areas where persons walk along.
- Set up beam targets (e.g. black V-shaped material).
- Shield reflections which go beyond the experiment.

Equipment

Scope of delivery

Item	Quantity
Alignment laser with holder:	
- Frequency doubled green alignment laser (0.2 / 1 mW)	1
Optical bench on carrier rail 1500 mm	1
Diaphragms for laser alignment	2
Slide mount for optical bench	3
Holder for D = 25.4 mm with xy-fine adjustment	2
Dielectric laser mirror for red light HR flat / flat	1
Dielectric laser mirror for red light HR R = 1400 mm / flat	1
Dielectric laser mirror for red light OC R = 1400 mm / flat	1
Dielectric laser mirror for red light HR R = 1000 mm / flat	1
He-Ne laser tube in adjustable holder	1
Power supply for He-Ne lasers, 4 kV continuous / 12 kV ignition, 4...10 mA	1
Connecting cable, 4 mm plug, 32 A, green-yellow, 2000 mm	1

Table 19: Equipment for labwork 06.

Accessories

Accessories	Code
Protective glasses for He-Ne laser	08581.10
Danger sign –LASER–	06542.00
Screen, 150 mm x 150 mm	09826.00
Cleaning set for lasers	08582.00
Photo element, silicon	08734.00
Digital multimeter	07128.00
Lyot plate on carrier and slide mount	08656.10
Littrow prism on carrier and slide mount	08656.20
Fabry-Perot etalon on carrier and slide mount	08656.30
He-Ne laser advanced experimental set containing Lyot plate, Littrow prism, and Fabry-Perot etalon	08656.02

Table 20: List of accessories

Waste disposal

The packaging consists predominately of environmental compatible materials that can be passed on for disposal by the local recycling service.

6.2 Setup and Procedure

Adjustment of the alignment laser

Place the optical bench on a plane and stable surface. Adjust the leveling screws in a way that the optical bench stands firmly.

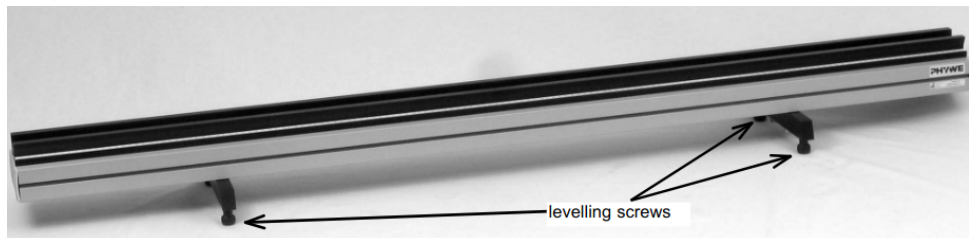


Figure 46: Levelling screws of the optical bench.

Mount the alignment laser on the left end of the optical bench and insert the diaphragm in front of the laser with the label "left" facing the laser. Turn on the alignment laser. Loosen the grub screws on the adjustment screws of the alignment laser and position the laser so that the green laser beam passes the hole in the left diaphragm (Figs. 47, 48). Put the diaphragm with the label "right" on a slide mount on the right end of the optical bench.

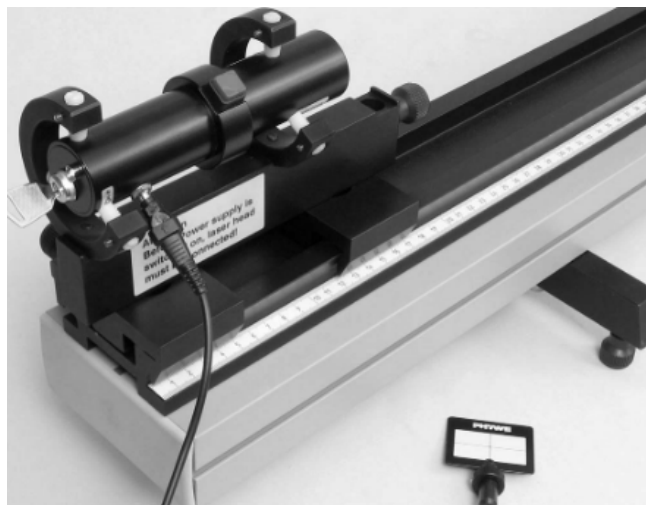


Figure 47: Alignment laser.

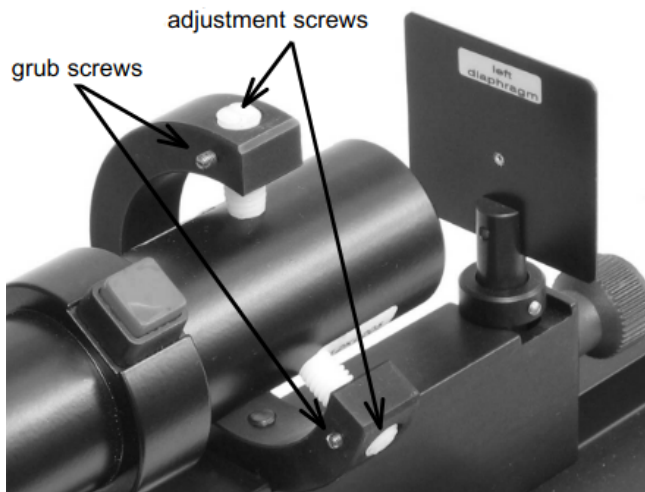


Figure 48: Adjustment screws.

Adjust the green laser's position so that the beam passes exactly through the middle of the right diaphragm – the hole of the diaphragm in the centre of the beam (Figs. 49, 50). Don't loosen the ring on the diaphragms – it is adjusted by the manufacturer such that the holes in the diaphragms have exactly the same height.

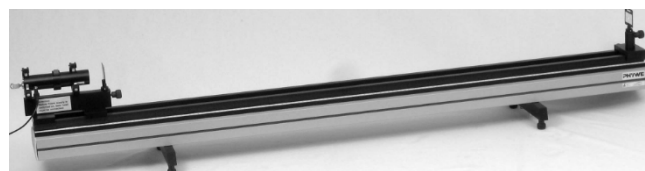


Figure 49: Adjusting the alignment laser.

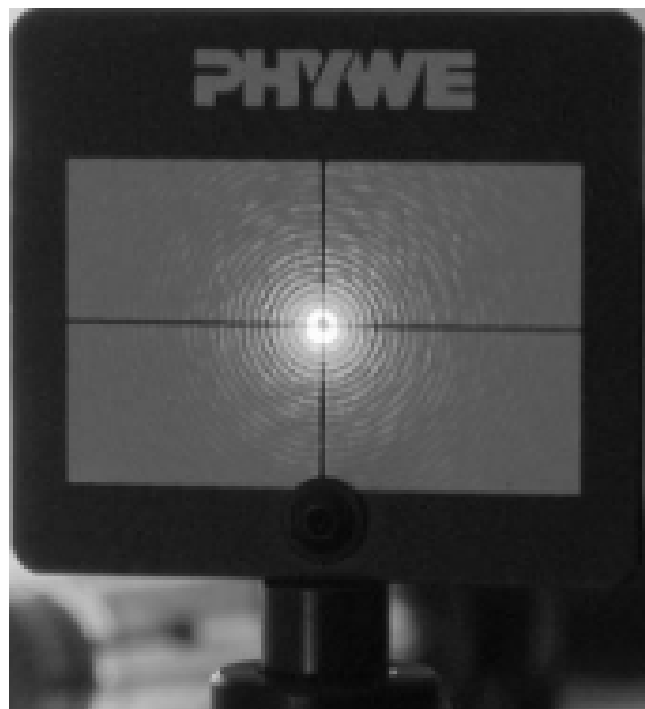


Figure 50: Correct adjustment.

Adjustment of the laser tube

Mount the laser tube with it's holder onto the optical bench and connect both ground and high-voltage cable to it's power supply (Fig. 51).

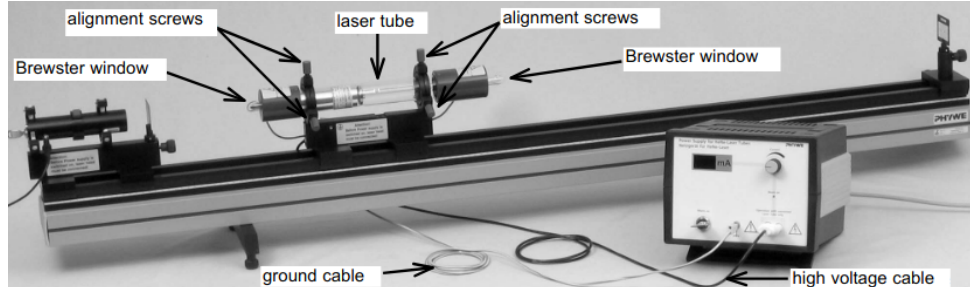


Figure 51: Mounting the laser tube.

Position the tube with the alignment screws in a way that the alignment beam passes the centre of both Brewster windows and does not touch the inner tube. The light spot on the right diaphragm has to be undistorted and should not be surrounded by reflections (Fig. 52). No reflection should be visible on the left diaphragm.

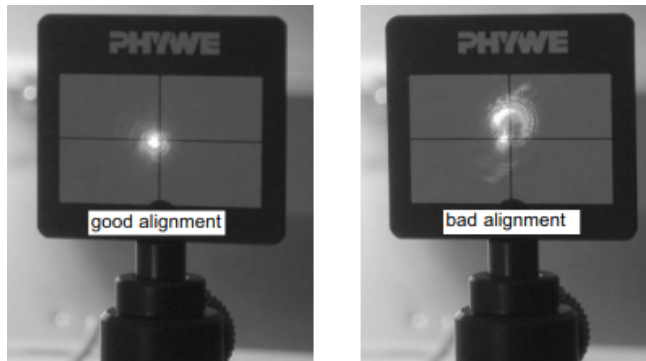


Figure 52: Adjustment of the laser tube.

In case a precise alignment of the laser beam is necessary for following experiments, the He-Ne laser beam may be readjusted by "beam walking" later on so that the beam impinges upon the middle of the right diaphragm again.

Adjustment of the right resonator mirror

Take the concave high reflective mirror (high reflective = HR, out coupling = OC) with 1000 mm radius (HR flach/1000 mm) and insert it into a xy-adjusting support on a slide mount.

The labeled side of the mirror is the high reflective concave one and has to face the laser tube (Fig. 53).

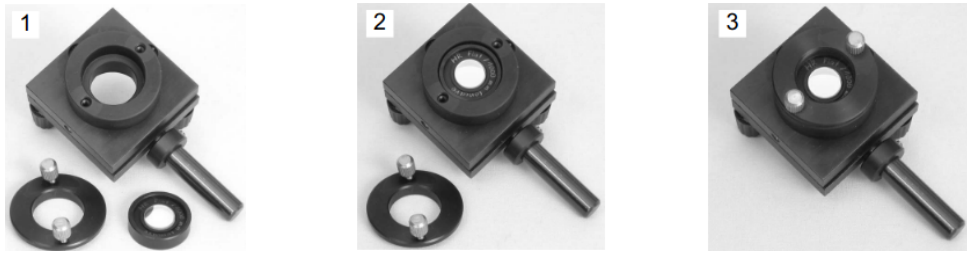


Figure 53: Assembling the resonator mirror.

Adjust the mirror in a way that the light spot of the reflection of the adjustment laser on the left diaphragm is undistorted and precisely in the centre.

There may be two reflection spots visible – one from the concave front side and one reflection of the back of the mirror. They may be distinguished by their size. Which of them has the bigger size depends on the distance between mirror and diaphragm – the focal length of a mirror with 1000 mm radius is 500 mm – so moving the mirror along the optical bench will reveal the correct spot. The reflex of the concave front side of the mirror is the one that has to be centered precisely. For starting a laser in a hemispheric resonator cavity, start with a mirror spacing less than ca. 70% of the radius of the concave mirror and the laser tube near the flat mirror.

Adjustment of the left resonator mirror

Take the flat high reflective mirror (HR flach/flach) and insert it into a xy-adjusting support on a slide mount. The labeled side of the mirror is the high reflective one and has to face the laser tube.

Adjust the mirror in a way that the light reflex of the adjustment laser on the left diaphragm is undistorted and precisely in the centre (Fig. 54).

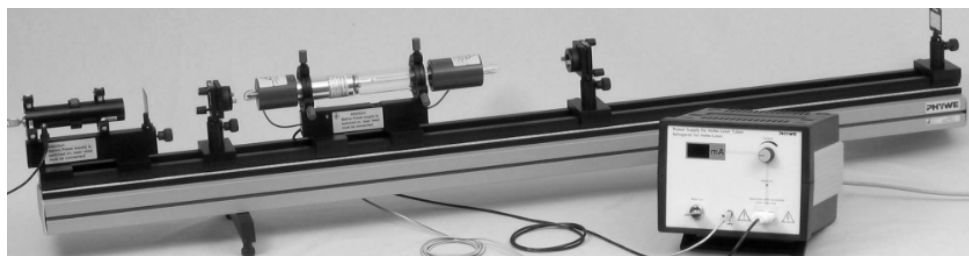


Figure 54: Left resonator mirror.

Starting the laser process

Turn on the He-Ne laser power supply with the key switch and set the tube current to 6.5 mA.

Wobble the adjustments screws on the right resonator mirror – one of them slowly and the other one faster – scanning the xy-range. E.g. keeping an eye on the alignment beam reflection on the left diaphragm turn the screw for horizontal adjustment of the right hand mirror very slowly first to the right and then to the left side of the assumed centre position while turning

the screw for vertical adjustment fast up and down from the assumed centre position. When a laser flash is seen, optimize the laser power by readjusting both mirrors and the tube position. Repeat the optimization process readjusting all the components.

If the laser process starting position can not be found, check on all the adjustments made before. Check the cleanliness of the optical components. If the laser still does not ignite, disassemble the set-up and start the adjustment over again.

If the set-up of the laser is changed, e.g. the laser is to be moved along the optical bench, all changes have to be done step by step: Perform a change on one component only and then start the laser process and optimize the output power of the laser before you alter another component. Otherwise it might be hard to find a position where the laser starts if more than one component is maladjusted.

Readjustment of the alignment of the laser beam is done by "beam walking" mentioned before. If the output power is already optimized, the left resonator mirror is turned in the direction that the light spot moves in the desired direction as far as possible without extinguishing the laser. Then the output power is raised again readjusting the left mirror and the laser tube position. This procedure is repeated until the desired position is achieved.

Cleaning the optical components

Optimal cleanliness of the Brewster windows and the resonator mirrors is the precondition for optimal output power and stable continuous operation of the He-Ne laser and thus correct measurement results. The high electric field strength inside the resonator may support the adhesion of dust.

The optical surfaces are coated and the coating is sensitive to touching and scratching and can easily be damaged. They must not get in contact with hard objects and may not be touched with the fingers. Optical instruments are fragile and have to be handled with care.

The cleaning has to be carried out with caution and may be done in the following way:

Acetone, a syringe, plastic tweezers and a lens cleaning tissue are taken from the PHYWE cleaning set for lasers Nr. 08582.00. The syringe is filled with some acetone.

A lens cleaning tissue is cut into half (Fig. 55). Wash your hands before touching the tissue – touch it as few as possible and especially not in the region that is to get in contact with the optical surfaces.

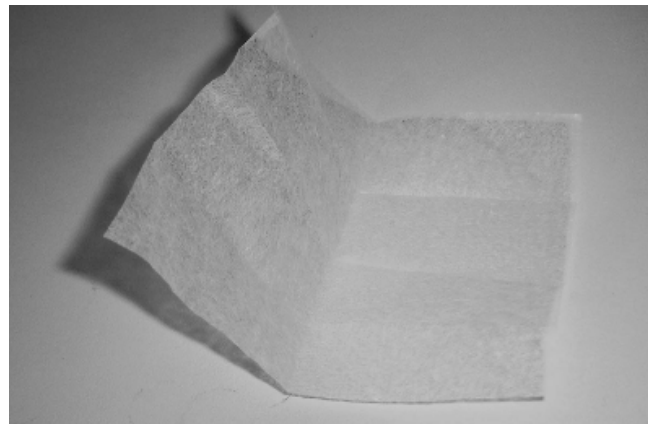


Figure 55: Cleaning tissue

The half tissue is folded to 1 cm x 3 cm. The folded tissue is held by the plastic tweezers. Some drops of acetone are dripped with the syringe onto the tissue. Excess acetone is removed by shaking the tissue. The optical surfaces are wiped with the tissue without the tweezers touching them. Wipe only in the indicated direction (Fig. 56).

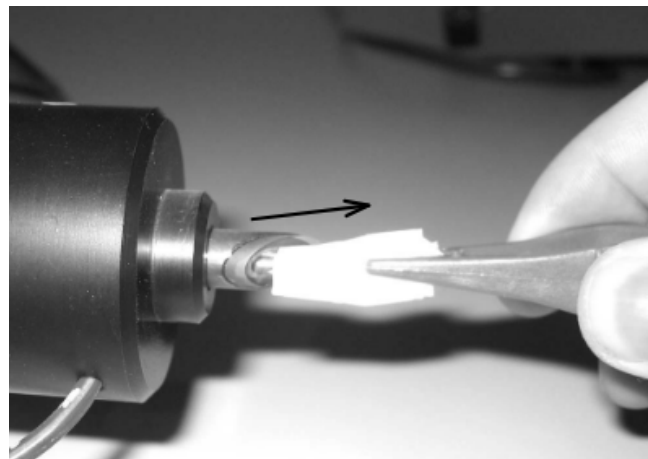


Figure 56: Cleaning the brewster window.

Acetone may dissolve plastic, varnish, synthetics and adhesives. So bring only the optical surfaces you want to clean in contact with acetone!

6.3 Theory and Evaluation

Introduction

The Helium-Neon laser was the first continuous laser. It was invented by Javan et al. in 1961 and is still in widespread use. Javan's first He-Ne laser oscillated at a wavelength of 1.5 μm , since the amplification at this wavelength is considerably higher than at the red 632.8 nm line which is nowadays commonly used. The first red He-Ne laser was built one year later by White and Ridgen.

The similarity between the manufacturing techniques of He-Ne lasers and electron valves helped in the mass production and distribution of He-Ne lasers.

He-Ne lasers will have to increasingly compete with laser diodes in the future. But He-Ne lasers are still unequalled as far as beam geometry and purity of modes are concerned. Laser diodes will have to be improved to a great extent before they pose a serious threat to He-Ne lasers.

Light amplification

Light amplification is possible by stimulated emission of radiation. For the possibility of stimulated emission exceeding the light, a population inversion of two energy states with an optical transition between them is necessary, i.e., there have to be more states occupied in the higher energy level than in the lower one. So only systems far away from thermodynamic equilibrium may possibly be amplifiers. For continuous lasers, at least three states are involved in the process.

Feedback turns an amplifier into an oscillator. An amplifier together with a resonator with a resonance frequency inside the frequency range where the gain of the amplifier exceeds unity represents a stabilized oscillator. In the case of gas lasers, the gain profile of the amplifier is the Doppler broadened line profile of the optical transition. The optical resonator modes are the standing waves that are possible in an optical cavity consisting of some mirrors.

The principle underlying stimulated emission of photons is Bose-Einstein statistics. While for fermions it is strictly forbidden to occupy the same quantum state (exchanging two fermions in a multi-particle state reverses the sign of the wave function), for bosons, it is more likely to be found in a state that is already highly populated. So a system with population inversion releases its photons into an already crowded resonator mode—the resonator mode completely occupying the photon state (quantum numbers e.g., the TEM_{mn} numbers).

He-Ne Energy-level diagram

The fascination for inert gases and their clear atomic structure formed the basis for many spectroscopic investigations. The knowledge of the spectroscopic data was extremely helpful in deciding to choose helium and neon for the first lasers, using the criterion of Schawlow and Townes from 1958 to estimate whether a population inversion was feasible for laser operation. The lifetime of the s - and p -states were well known. The s -states were 10 times longer than those of the p -states. The inversion condition can therefore be fulfilled.

Fig. 57 shows the reduced energy-level diagram for helium and neon. Only those levels important in the discussion of the excitation and laser processes at a wavelength of 632 nm are indicated.

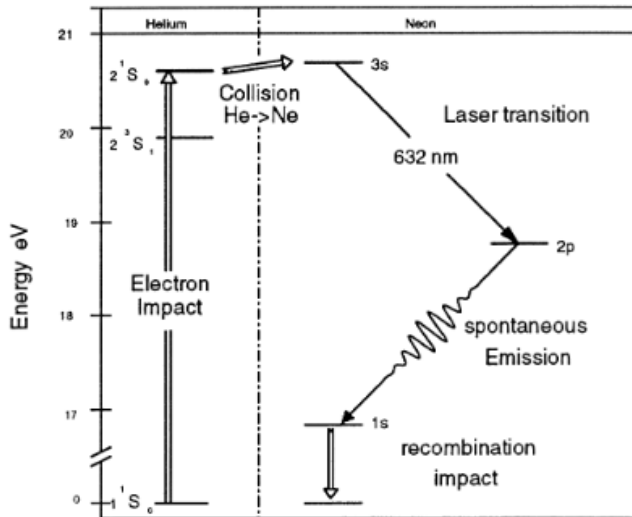


Figure 57: Excitation and laser process for the visible laser emission.

The left side of the representation shows the lower levels of the helium atom. Note that the energy scale is interrupted and that there is a larger difference in energy in the recombination process than is evident in the diagram. Paschen's names for the neon energy levels are used (Racah's term descriptions are often found as well). The terms are simply numbered consecutively, from bottom to top. A characteristic of helium is that its excited states with lowest energy, 2^3S_1 and 2^1S_0 , are metastable, i.e., optical transitions to the ground state 1^1S_0 are not allowed because of the selection rules for optical transitions. These excited states are populated by electron collisions in a gas discharge (collisions of the second type, Fig. 58).

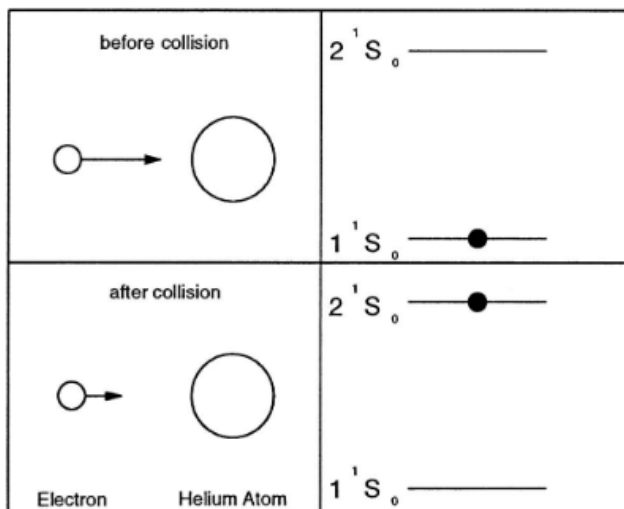


Figure 58: Electron collision of the second kind.

A collision is called a collision of the second type if the internal energy of the colliding particles is changed in the reaction, e.g., a transition from one energy state to another of one or both of the particles takes place. Apart from the electron collision of the second type, there is also the atomic collision of the second type. In the latter, an excited helium atom state decays without photon emission by transferring energy to a neon atom which is then excited. Both

these processes form the basis for the production of a population inversion.

If we look at Fig. 57, we can see that the 2^1S_0 level of Helium is slightly below the $3s$ level of neon. However, the additional thermal energy kT is sufficient to overcome this gap.

As already mentioned, the lifetime of the s -states of the neon is approximately 10 times longer than the one of the p -states. An immediate population inversion between the $3s$ and $2p$ levels will therefore be generated. The $2s$ level is emptied due to spontaneous emission into the $1s$ level. This state decays into the ground state primarily through collisions with the tube wall (capillary), since an optical transition is not allowed. This process is the bottleneck in the laser cycle. It is therefore advisable to choose a capillary diameter that is as small as possible. On the other hand, an active volume as big as possible is desirable for high output power. Modern He-Ne lasers work at an optimum of these contradictory conditions. This bottleneck is the main reason for the comparatively low output of He-Ne lasers.

We have discussed the laser cycle of the commonly known red line at 632 nm up to this point. However, the neon has several other transitions, used to produce about 200 laser lines in laboratories. The following explanation describes the energy-level diagram for further visible lines. That infrared laser light is also possible.

The $3s$ state of Neon is populated by Helium atoms of the 2^1S_0 state as a result of atomic collisions with Neon atoms in the ground state. The $3s$ state consists of 4 sub-states. Of these, it is primarily the $3s_2$ state that has been populated through the collision process. The population density of the other $3s$ sub-states is approximately 400 times less than that of the $3s_2$ state. The $2s$ state is populated with Helium atoms in the 2^1S_0 state, as a result of an atomic collision.

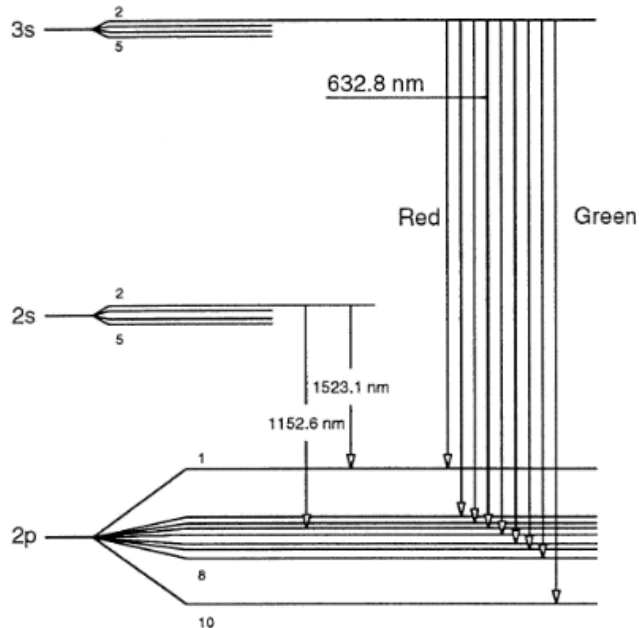


Figure 59: The most important laser transitions in the neon system.

The four sub-states of the $2s$ group are all populated in a similar way. Visible (VIS) optical transitions and laser processes are taking place between the $3s_2 \rightarrow 2p$, and infrared (IR) between

the $2s_2 \rightarrow 2p$ energy levels.

Table 21 shows the most important laser transitions. The Einstein coefficients A_{2s} are given for the visible lines, and amplification is indicated as percentage per meter.

Further laser transitions are known, which start at the $3s_2$ level and extend at the $3p$ level of neon. However, these laser transitions are even further within the infrared spectral range, and dielectric resonator mirrors for visible light are not suitable for infrared light. Those transitions are not particularly suitable for experiments. Notice that these lines originate from the same level as the visible lines and are therefore competing with them. Since the cross-section of the stimulated emission is increasing with λ^3 as well, the amplification of these lines is therefore very strong. This applies to the $3.39 \mu\text{m}$ line in particular, which in the case of a sufficiently long capillary may show laser activity (so-called superfluorescence) even without an optical resonator.

Light amplification profile of the neon atoms

The Neon atoms move more or less freely in the laser tube but at different speeds. The number N of neon atoms within the mass m , within a speed interval of v to $v+dv$, is described according to the Maxwell-Boltzmann distribution:

$$\frac{n(v_x)}{N} = \frac{4}{\sqrt{\pi}} \sqrt{\frac{2kT}{m}} e^{-\frac{mv^2}{kT}} dv_x \quad (46)$$

where T is the absolute temperature and k is Boltzmann's constant. The above equation is applicable for all directions in space.

However, we are only interested in the distribution of speed in the direction of the capillary. Using $v^2 = v_x^2 + v_y^2 + v_z^2$, we obtain for the direction x :

$$\frac{n(v_x)}{N} = \frac{4}{\sqrt{\pi}} \sqrt{\frac{2kT}{m}} e^{-\frac{mv^2}{kT}} dv_x \quad (47)$$

A resting observer will now see the absorption or emission frequency shifted, due to Doppler's effect (Ch. Doppler: Abh. d. K. Boehmischen Ges. d. Wiss. (5). Vol.11 (1842) P.4b5), and the value of the shift will be:

$$f = \frac{f_0}{1 \pm v/c} \quad (48)$$

assuming $v \ll c$.

- (1) Possible laser transitions if laser tube is supplied with perpendicular or Brewster windows.
- (2) Possible laser transitions if laser tube is supplied with Brewster windows and special set of mirrors.
- (3) Possible laser transitions if laser tube is supplied with Brewster windows and IR mirror set.
- (*) Transition not allowed.

Transition	Wavelength (nm)	Gain (%/m)
$3s_2 \rightarrow 2p_1$	730.5	12
$3s_2 \rightarrow 2p_2$	640.1	4.3
$3s_2 \rightarrow 2p_3$	635.2	1.0
$3s_2 \rightarrow 2p_4$	632.8	10.0
$3s_2 \rightarrow 2p_5$	629.4	1.9
$3s_2 \rightarrow 2p_6$	611.8	1.7
$3s_2 \rightarrow 2p_7$	604.6	0.6
$3s_2 \rightarrow 2p_8$	539.9	0.5
$3s_2 \rightarrow 2p_9$		
$3s_3 \rightarrow 2p_{10}$	543.3	0.52
$2s_2 \rightarrow 2p_1$	1523.1	
$2s_2 \rightarrow 2p_2$	1177.0	
$2s_2 \rightarrow 2p_3$	1160.5	
$2s_2 \rightarrow 2p_4$	1152.6	
$2s_2 \rightarrow 2p_5$	1141.2	
$2s_2 \rightarrow 2p_6$	1084.7	
$2s_2 \rightarrow 2p_7$	1062.3	
$2s_2 \rightarrow 2p_8$	1029.8	
$2s_2 \rightarrow 2p_9$		
$2s_2 \rightarrow 2p_{10}$	886.5	
$2s_3 \rightarrow 2p_2$	1198.8	
$2s_3 \rightarrow 2p_5$	1161.7	
$2s_3 \rightarrow 2p_7$	1080.1	

Table 21: Transitions and laser lines

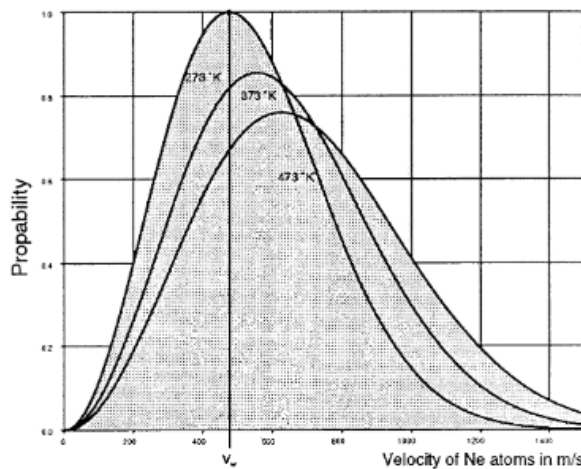


Figure 60: Maxwell-Boltzmann speed distribution.

f_0 is the absorption or emission frequency of the resting neon atom and c the speed of light.

If the Doppler equation (2) is used to substitute the velocity v in the Maxwell-Boltzmann's velocity distribution (1), the line broadening produced by the movement of neon atoms can be found. Since the intensity is proportional to the number of absorbing or emitting neon atoms, the intensity distribution will be:

$$I(f) = I(f_0) \cdot e^{-\frac{f-f_0}{f_0 \cdot v_m}} \quad (49)$$

with v_m , the most likely speed,

$$v_m = \sqrt{\frac{2kT}{m}} \quad (50)$$

The full width at half maximum is calculated by setting $I(v) = \frac{1}{2}I(v_0)$ and the result is:

$$\Delta f_{\text{Doppler}} = \sqrt{4 \ln 2} \cdot \frac{v_m}{c} f_0 \quad (51)$$

We can conclude from (4) that the line broadening caused by Doppler's effect is larger in the case of:

- higher resonance frequencies f_0 ,
- smaller wavelengths $f_0 = c/\lambda_0$ (UV-lines),
- higher most likely velocity v_m , meaning higher temperature T .

And smaller in the case of:

- a larger particle mass.

The line profile also corresponds to a Gaussian distribution curve. Fig. 61 shows this kind of profile. The histogram only approaches the distribution curve when the speed intervals dv are small.

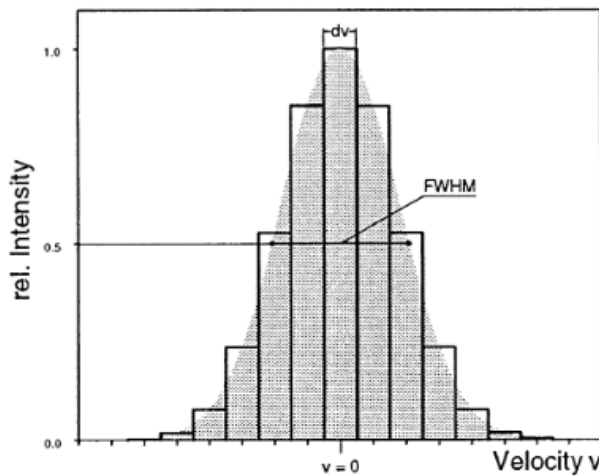


Figure 61: Inhomogeneous line profile, speed intervals dv .

On closer observation, we can see that a line broadened by the Doppler effect actually does not have a pure Gaussian distribution. The natural linewidth due to the lifetime of the state has to be taken into account. Consider an ensemble of Ne atoms with speed components of value v in

the direction we are looking at. All these atoms emit light not only with the same frequency f or wavelength λ but their emission lies in the range of the natural linewidth of the transition. The shorter the lifetime, the broader the emission line profile (time-energy uncertainty). The population n_2 of a state 2 decays spontaneously into a state 1 with lower energy with a time constant τ_s , following the equation:

$$n_2(t) = n(t=0)e^{-A_{21}t}, \quad \text{with } \tau_s = \frac{1}{A_{21}} \quad (52)$$

where A_{21} is the Einstein coefficient for spontaneous emission.

The ensemble of Ne atoms then emits a frequency spectrum represented by a Lorentz profile:

$$\delta(f) = \frac{1}{4\pi} \cdot \frac{1}{(f - f_{21})^2 + (1/2 \cdot \tau_s)^2}, \quad f_0 = f_{21} \quad (53)$$

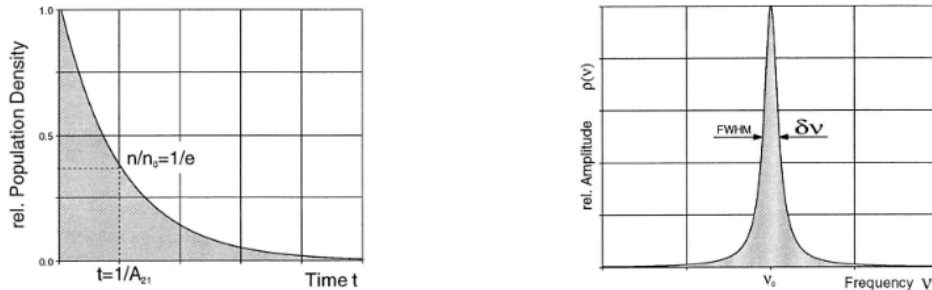


Figure 62: Decay of the population of state 2 into state 1 and natural linewidth.

The exact profile can be determined from the convolution of the Gaussian profile with the individual Lorentz profiles. The result obtained in this manner is called the Voigt profile. Since one group of particles in an ensemble can be assigned to a given speed v , these groups have characteristics that make them distinguishable. Every group has its own frequency of resonance. Which group a photon interacts with depends on the energy (frequency) of the photon. This does not affect the other groups which are not resonant on this interaction. Therefore, such kind of a gain profile is termed inhomogeneous.

Gain occurs in a medium when it shows inversion. This means that the population density of the upper level n_2 (3s in the Ne-system) is larger than the population density of the lower state n_1 (2p). Transition can only take place between sub-ensembles that have the same velocity v because the optical transition does not change the speed of the particular Ne atom. Besides some specific other constants, the gain is proportional to the difference $n_2 - n_1$. Now, we place the inverted ensemble of Ne atoms into an optical cavity, which is formed by two mirrors having the distance L . Due to spontaneous emission, photons are generated, which will be amplified by the inverted medium and reflected back from the mirrors, undergoing a large number of passes through the amplifying medium. If the gain compensates for the losses, a standing laser wave will build up inside the optical resonator.

Such a standing wave is also termed the oscillating mode of the resonator, also called an eigenmode or simply mode. Every mode must fulfill the following condition because of field constraints on the surfaces of the mirrors:

$$L = n \cdot \frac{\lambda}{2} \quad \text{or} \quad L = n \cdot \frac{c}{2f} \quad (54)$$

where L represents the length of the resonator, λ the wavelength, c the speed of light, f the frequency of the generated light, and n an integer number.

Thus, every mode has its frequency:

$$f(n) = n \cdot \frac{c}{2L} \quad (55)$$

For example, a He-Ne-Laser with a resonator length of 30 cm at an emission wavelength of 632.8 nm will have the following value for n :

$$n = \frac{c}{\lambda} \cdot 2L = \frac{0.3}{632.8 \times 10^{-9}} \approx 950000 \quad (56)$$

The difference in frequency between two neighboring modes is:

$$\Delta f = f(n+1) - f(n) = (n+1) \cdot \frac{c}{2L} - n \cdot \frac{c}{2L} = \frac{c}{2L} \quad (57)$$

Using the above example, the frequency difference between modes would be:

$$\Delta f = \frac{3 \times 10^8 \text{ m/s}}{2 \times 0.3 \text{ m}} = 5 \times 10^8 \text{ Hz} = 500 \text{ MHz} \quad (58)$$

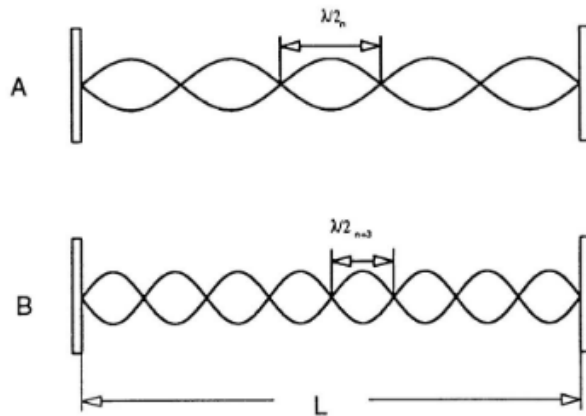


Figure 63: Standing longitudinal waves in an optical resonator. A with n nodes and B with $n+3$ nodes.

If the active laser material is now brought into the resonator, standing waves will be formed, and energy will be extracted from the material. However, the resonator can only extract energy for which it is resonant. The resonator has an indefinite amount of modes, whereas the active material only emits in an area of frequency determined by the emission line width.

Fig. 64 shows the situation in the case of material with a line that is inhomogeneously broadened.

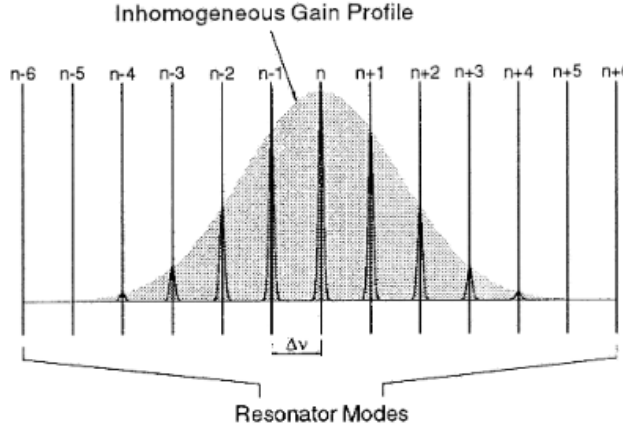


Figure 64: Inhomogeneous gain profile (Gaussian profile) interacting with an optical resonator.

If the laser is operating in a steady state, it may emit in several longitudinal modes. Since only the modes within the emission profile may be amplified and the frequency difference of the modes depends on the resonator length, the number of oscillating modes increases with the resonator length. Single-mode He-Ne lasers usually have a resonator length of only 12.7 cm (5 inches). Since the modes are fed by an inhomogeneous emission profile, they can also exist independently.

Resonators

In the following section, some fundamentals useful in the description and calculation of optical resonators will be introduced. Stability diagrams, the beam radius, and beam sizes for the resonator types used in later experiments will be calculated and discussed. The investigations and calculations will be carried out for an empty resonator, ignoring particular influences on the characteristics of the resonator (e.g., thermal lenses, abnormal refractive index, etc.).

The ABCD law will be introduced and used in this context. Just like the Jones matrix formalism, the type of optical calculation is an elegant method for solving optics (ray tracing) in a complex optical system. Fig. ?? shows that an equivalent lens system can be an equivalent to an optical resonator. The beam path of the resonator can be traced using the ABCD law, aided by an equivalent lens system.

First, we must presume that the following calculations are correct for the limits of geometric optics. Additionally, the beam angle is $< 15^\circ$ to the optical axis, so $\alpha \approx \epsilon$ is valid. This is fulfilled for laser resonators. A light beam is clearly defined by its height X to the optical axis and the slope at this point.

Beams in an optical resonator have to pass through the same optical structure several times. After passing through it n times, the ABCD law for a particular place Z of the lens guide (Fig. 65) would be:

$$\begin{pmatrix} X_f \\ \alpha_f \end{pmatrix} = \begin{pmatrix} A & B \\ C & D \end{pmatrix}^n \begin{pmatrix} X_i \\ \alpha_i \end{pmatrix} \quad (59)$$

In this case, the ABCD matrix is the equivalent lens guide given to the resonator. The n -th power of a 2×2 matrix is calculated as follows:

$$\begin{pmatrix} A & B \\ C & D \end{pmatrix}^n = \frac{1}{\sin(\theta)} \begin{pmatrix} a & b \\ c & d \end{pmatrix} \quad (60)$$

where:

$$\begin{aligned}\theta &= \arccos((A + D)/2) \\ a &= A \sin(n\theta) - \sin((n - 1)\theta) \\ b &= B \sin(n\theta) \\ c &= C \sin(n\theta) \\ d &= D \sin(n\theta) - \sin((n - 1)\theta)\end{aligned}$$

The trace of the above ABCD matrix $|A + D|$ has to be less than or equal to one if the beams are to remain within the lens guide. So the criterion of stability for the lens guide, and therefore also for the accompanying resonator, is:

$$|A + D| \leq 1 \quad (61)$$

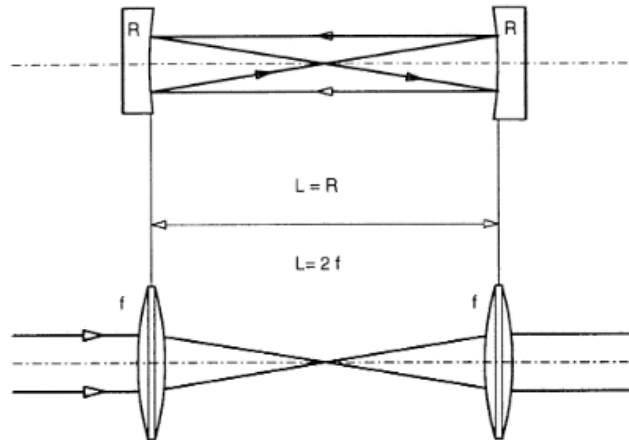


Figure 65: Spherical resonator with equivalent lens guide.

An equivalent lens guide system can be linked to every resonator. The ABCD matrix may be determined for this optical structure (several simple lenses). The stability diagram for the different mirror configurations with given mirror radii can easily be calculated.

For a resonator with:

- Radius of curvature of left mirror: b_1
- Radius of curvature of right mirror: b_2
- Resonator length: d

We define:

$$g_i = 1 - \frac{d}{b_i} \quad (62)$$

Then the criterion of stability is:

$$0 < g_1 g_2 < 1 \quad (63)$$

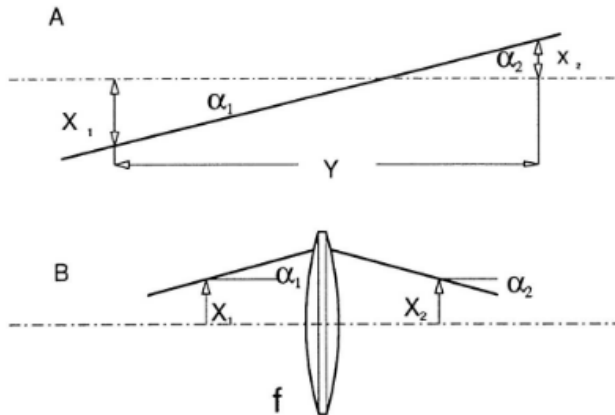


Figure 66: A: Light beam with characteristic sizes. B: Trace through a lens.

Type	Mirror Radius	Stability Parameter
Confocal	$b_1 + b_2 = 2d$	$g_1 g_2 = 2g_1 g_2$
Concentric	$b_1 = b_2 = d$	$g_1 g_2 = 1$
Symmetric	$b_1 = b_2$	$g_1 = g_2$
Symmetric Confocal	$b_1 = b_2 = 2d$	$g_1 g_2 = 1$
Symmetric Concentric	$b_1 = b_2 = \frac{1}{2}d$	$g_1 g_2 = 0$
Semi-Confocal	$b_1 = 2d, b_2 = \infty$	$g_1 = 1, g_2 = 1$
Plane	$b_1 = b_2 = \infty$	$g_1 = g_2 = 1$

Table 22: Some special types of resonators.

Laser tubes and brewster windows

Brewster windows have two functions. They hermetically seal the tube, as well as ensure that there is a definite polarization in laser oscillation without additional losses.

Brewster windows are soldered on to a special metal (Vacon). The tube being used has a ignition voltage of approx. 8 kV and an operating voltage of approx. 2 kV. The optimal current for the 632 nm line is 5 mA. The Brewster windows of the laser tube are arranged in a way that enables compensation for beam displacement by the windows.

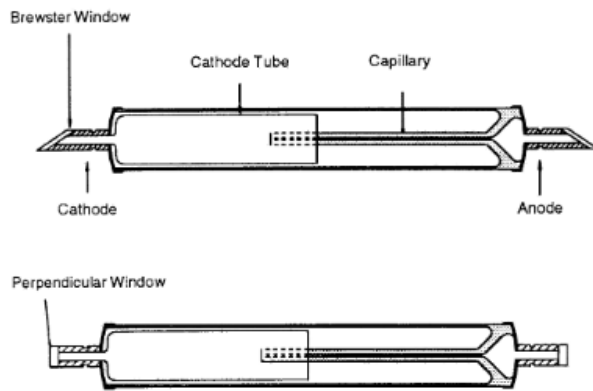


Figure 67: Laser tube with Brewster windows and perpendicular windows with highly anti reflection coating.

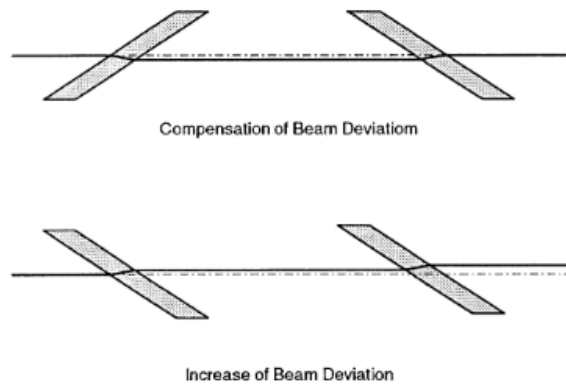


Figure 68: Two possible arrangements of Brewster windows.

6.4 Results and Discussion

Experiment setup



Figure 69: Practical set-up of experiment

The desired outcome of this helium-neon (He-Ne) laser setup experiment is to successfully achieve and optimize lasing action (laser emission) by properly aligning the optical components and establishing a stable laser resonator. Specific objectives include:

- Laser Construction and Operation: Assemble the helium-neon laser with proper alignment of optical components, ensuring the system produces coherent laser light at the desired wavelength (typically 632.8 nm in the visible spectrum)
- Optimization of Laser Output: Perform fine adjustments to maximize the laser's performance, including optimizing alignment, gain coefficient, and output power
- Exploration of Laser Properties: Investigate phenomena such as single longitudinal mode operation, frequency resolution, Doppler broadening, and energy transitions within the helium-neon gas mixture
- Experimental Applications: Use the laser for advanced experiments, such as studying optical cavity modes, measuring rotation rates via the Sagnac effect (in gyroscope setups), or analyzing specific wavelengths for scientific purposes

The experiment demonstrates the importance of systematic assembly and alignment in achieving lasing.

The helium-neon laser's reliance on quantum mechanical principles (e.g., selection rules) highlights its significance in understanding atomic transitions and energy levels.

Despite advancements like semiconductor lasers, He-Ne lasers remain relevant due to their reliability and precision in scientific applications